Institute of Theoretical and Applied Physics

Turunç - Marmaris - TURKEY

ISMFA - International School on Magnetohydrodynamics and Fusion Applications
09-16 September 2011

Plasma Focus Numerical Experiments

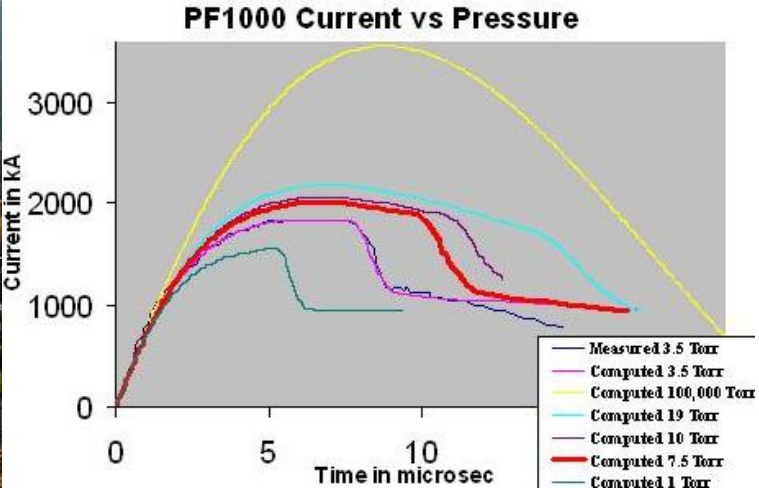

T.C. BAŞBAKANLIK DPT DEVLET PLANLAMA TEŞKİLATI

TÜBİTAK

IPFS Institute For Plasma Focus Studies
• Knowledge Should Be Freely Accessible To All •

INTI International University
LAUREATE INTERNATIONAL UNIVERSITIES

Plasma Focus Numerical Experiments
Basic Course

Sor Heoh Saw and **Sing Lee** in collaboration with **Erol Kurt**

Module 1: Introduction - The Plasma Focus and the Lee model

Summary

1.1 Description of the plasma focus; how it works, dimensions and lifetimes of the hot dense plasma
1.2 Scaling properties of the plasma focus
1.3 The radiative Lee model: the 5 phases
1.4 Using the Lee model as reference for diagnostics
1.5 Insights on plasma focus from numerical experiments using Lee model code

1.1 Description of the plasma focus. How it works, dimensions and lifetimes of the hot dense plasma

1.1.1 Introduction

The Plasma Focus is a compact powerful pulsed source of multi-radiation [1]. Even a small table- top sized 3 *kJ* plasma focus produces an intense burst of radiation with extremely high powers. For example when operated in neon, the x-ray emission power peaks at 10^9 *W* over a period of nanoseconds. When operated in deuterium the fusion neutron burst produces rates of neutron typically 10^{15} neutrons per second over burst durations of tens of nanosecond. The emission comes from a point source making these devices among the most powerful laboratory pulsed radiation sources in the world. These sources are plasma-based.

When matter is heated to a high enough temperature, it ionizes and becomes plasma. It emits electromagnetic radiation. The spectrum depends on the temperature and the material. The higher the temperature and the denser the matter, the more intense is the radiation. Beams of electrons and ions may also be emitted. If the material is deuterium, nuclear fusion may take place if the density and temperature are high enough. In that case neutrons are also emitted. Typically the temperatures are above several million *K* and compressed densities above atmospheric density starting with a gas a hundredth of an atmospheric density.

One way of achieving such highly heated material is by means of an electrical discharge through gases. As the gas is heated, it expands, lowering the density and making it difficult to heat further. Thus it is necessary to compress the gas whilst heating it, in order to achieve sufficiently intense conditions. An electrical discharge between two electrodes produces an azimuthal magnetic field which interacts with the column of current, giving rise to a self compression force which tends to constrict (or pinch) the column. In order to 'pinch', or hold together, a column of gas at about atmospheric density at a temperature of 1 million *K*, a rather large pressure has to be exerted by the pinching magnetic field. Thus an electric current of at least hundreds of *kA* are required even for a column of small radius of say 1 *mm*. Moreover the dynamic process requires that the current rises very rapidly, typically in under 0.1 μs in order to have a sufficiently hot and dense pinch. Such a pinch is known as a super-fast super-dense pinch; and requires special *MA* fast-rise (*ns*) pulsed-lines. These lines may be powered by capacitor banks, and suffer the disadvantage of conversion losses and high cost due to the cost of the high technology pulse-shaping line, in addition to the capacitor banks.

A superior method of producing the super-dense and super-hot pinch is to use the plasma focus. Not only does this device produce superior densities and temperatures, moreover its method of operation does away with the extra layer of technology required by the expensive and inefficient pulse-shaping line. A simple capacitor discharge is sufficient to power the plasma focus.

1.1.2 The plasma focus

The plasma focus is divided into two sections. The first is a pre-pinch (axial) section. The function of this section is primarily to delay the pinch until the capacitor discharge (rising in a damped sinusoidal fashion) approaches its maximum current. This is done by driving a current sheet down an axial (acceleration) section until the capacitor current approaches its peak. Then the current sheet is allowed to undergo transition into a radial compression phase. Thus the pinch starts and occurs at the top of the current pulse. This is equivalent to driving the pinch with a super-fast rising current; without necessitating the fast line technology. Moreover the intensity which is achieved is superior to the line driven pinch.

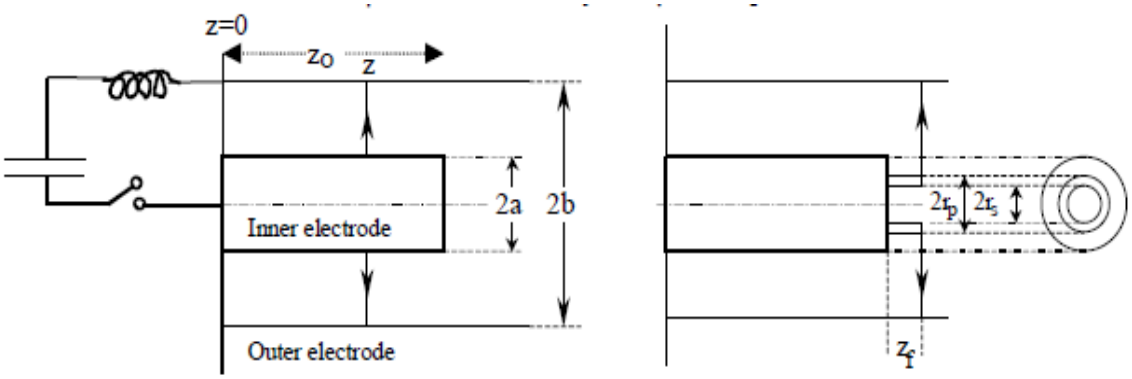

Figure 1. Schematic of the axial and radial phases. The left section depicts the axial phase, the right section the radial phase. In the left section, z is the effective position of the current sheath-shock front structure. In the right section r_s is the position of the inward moving shock front driven by the piston at position r_p. Between r_s and r_p is the radially imploding slug, elongating with a length z_f. The capacitor, static inductance and switch powering the plasma focus is shown for the axial phase schematic only.

The two-phase mechanism of the plasma focus [1] is shown in figure 1. The inner electrode (anode) is separated from the outer concentric cathode by an insulating backwall. The electrodes are enclosed in a chamber, evacuated and typically filled with gas at about 1/100 of atmospheric pressure. When the capacitor voltage is switched onto the focus tube, breakdown occurs axisymmetrically between the anode and cathode across the backwall. The 'sheet' of current lifts off the backwall as the magnetic field (B_θ) and it's inducing current (J_r) rises to a sufficient value.

Axial phase: The $J_r \; x \; B_\theta$ force then pushes the current sheet, accelerating it supersonically down the tube. This is very similar to the mechanism of a linear motor. The speed of the current sheet, the length of the tube and the rise time of the capacitor discharge are matched so that the current sheet reaches the end of the axial section just as the discharge reaches its quarter cycle. This phase typically lasts 1-3 μ*s* for a plasma focus of several *kJ*.

Radial Phase: The part of the current sheet in sliding contact with the anode then 'slips' off the end 'face' of the anode forming a cylinder of current, which is then pinched inwards. The wall of the imploding plasma cylinder has two boundaries (see figure 1 radial phase). The inner face of the wall, of radius r_s is an imploding shock front. The outer side of the wall, of radius r_p is the imploding current sheet, or magnetic piston. Between the shock front and the magnetic piston is the annular layer of plasma. Imploding inwards at higher and higher speeds, the shock front coalesces on-axis and a super-dense, super-hot plasma column is pinched onto the axis (see figure 2 [2]). This column stays super-hot and super-dense for typically ten *ns* for a small focus. The column then breaks up and explodes. For a

small plasma focus of several *kJ*, the most intense emission phase lasts for the order of several *ns*. The radiation source is spot-like (1*mm* diameter) when viewed end-on.

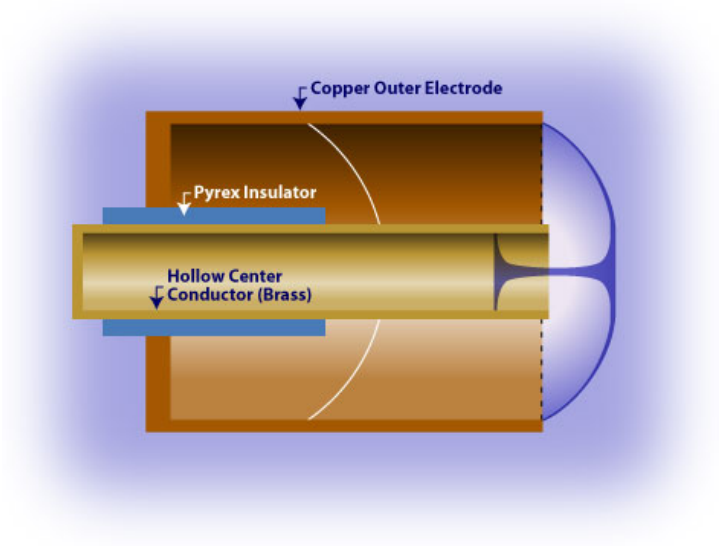

Figure 2. Dense plasma focus device. Image from Glenn Millam. Source: Focus Fusion Society For an animation of the plasma focus click here.

1.1.3 Radial dynamics of the plasma focus

Figure 3 shows a drawing of a typical plasma focus, powered by a single capacitor, switched by a simple parallel-plate spark-gap. The anode may be a hollow copper tube so that during the radial pinching phase the plasma not only elongates away from the anode face but also extends and elongates into the hollow anode (see figure 2). In figure 3 is shown the section where the current sheet is accelerated axially and also the radial section. Also shown in the same figure are shadowgraphs [3] taken of the actual radially imploding current sheet-shock front structure. The shadowgraphs are taken in a sequence, at different times. The times indicated on the shadowgraphs are relative to the moment judged to be the moment of maximum compression.

That moment is taken as t=0. The quality of the plasma compression can be seen to be very good, with excellent axisymmetry, and a very well compressed dense phase. In the lower left of figure 3 are shown the current and voltage signatures of the radial implosion [4], occurring at peak current. The implosion speeds are measured and observed to have a peak value approaching 30 *cm*/μ*s*.

This agrees with modelling, and by considering shock wave theory together with modelling [5] of subsequent reflected shock wave and compressive effects, a temperature of 6 million *K* (0.5 *keV*) is estimated for the column at peak compression, with a density of 2×10^{19} ions per cm^3. The values quoted here are for the UNU/ICTP PFF 3 *kJ* device.

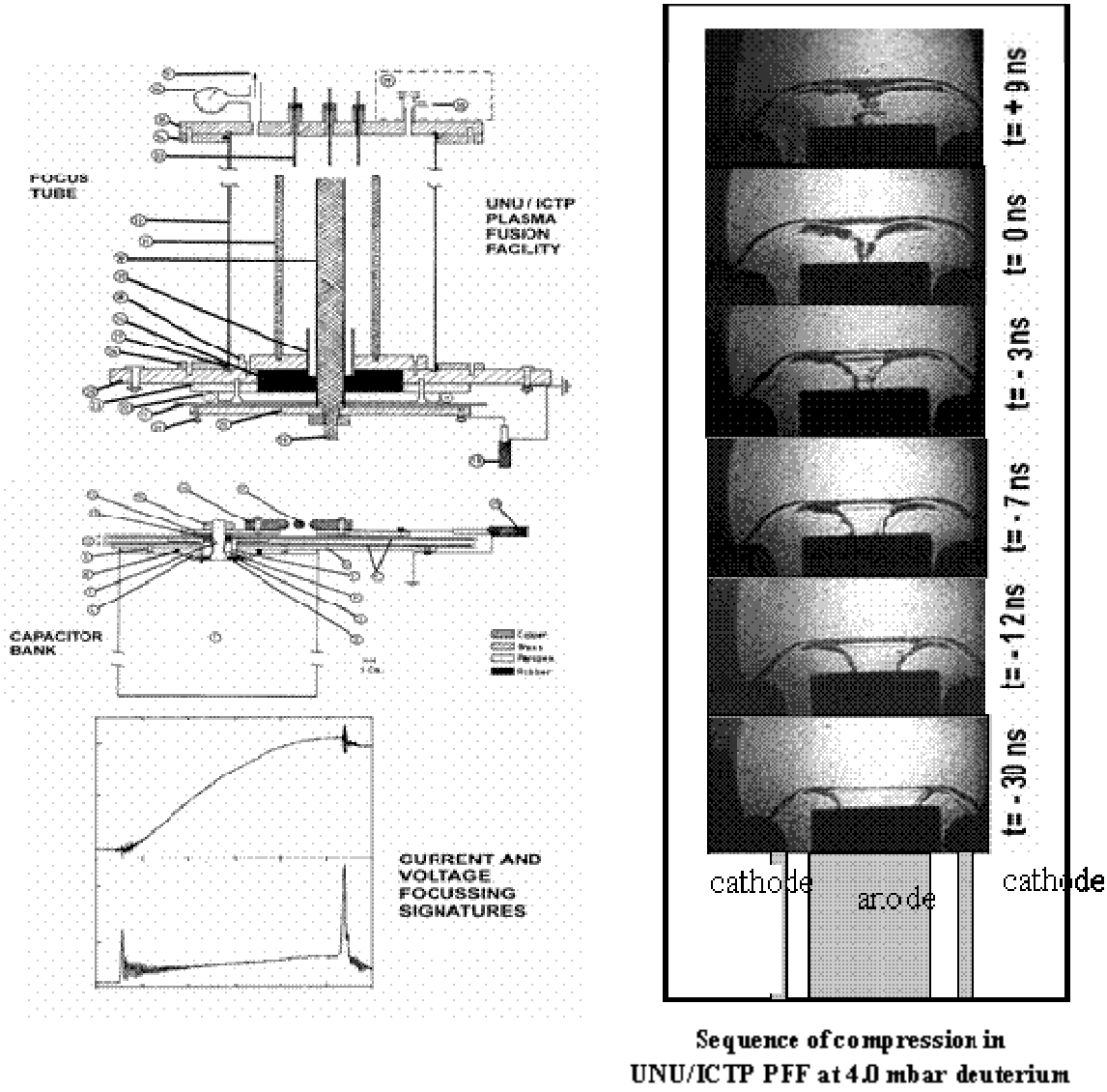

Figure 3. UNU/ICTP PFF - Design, Signatures and Dynamics

1.2 Scaling properties of the plasma focus

1.2.1 Various plasma focus devices

In figure 4a is shown the UNU ICTP PFF 3 *kJ* device [4-6] mounted on a 1 *m* by 1 *m* by 0.5 *m* trolley, which was wheeled around the International Centre for Theoretical Physics (ICTP) for the 1991 and 1993 Plasma Physics Colleges during the experimental sessions. The single capacitor is seen in the picture mounted on the trolley. In contrast, figure 4b shows the PF1000, the 1 *MJ* device [7] at the International Centre for Dense Magnetised Plasmas (ICDMP) in Warsaw, Poland. Only the chamber and the cables connecting the plasma focus to the capacitors are shown. The capacitor bank with its 288 capacitors, switches and chargers are located in a separate hall.

Figure 4a. 3kJ UNU ICTP PFF **Figure 4b.** 1 MJ PF1000 plasma focus

We show here the characteristics of several plasma focus devices [7].

Table 1 Characteristics of three plasma focus devices

Plasma Focus Devices	E_0 (kJ)	a (cm)	Z_0 (cm)	V_0 (kV)	P_0 (Torr)	I_{peak} (kA)	v_a (cm/us)	ID (kA/cm)	SF [(kAcm^{-1}) Torr$^{0.5}$]	Y_n (10^8)
PF1000	486	11.6	60	27	4	1850	11	160	85	1100
UNU ICTP PFF	2.7	1.0	15.5	14	3	164	9	173	100	0.20
PF400J	0.4	0.6	1.7	28	7	126	9	210	82	0.01

In table 1 we look at the PF1000 and study its properties at typical operation with device storage at 500 *kJ* level. We compare this big focus with two small devices at the *kJ* level.

From table 1 we note:

Voltage and pressure do not have any particular relationship to E_0.
Peak current I_{peak} increases with E_0.
Anode radius '*a*' increases with E_0.
ID (current per *cm* of anode radius) I_{peak}/a is in a narrow range from 160 to 210 *kA*/*cm*
SF (speed or drive factor) $(I_{peak}/a)/P_0^{0.5}$ is 82 to 100 $kAcm^{-1}/Torr^{0.5}$ deuterium gas [8].
Peak axial speed v_a is in the narrow range 9 to 11 *cm*/*us*.
Fusion neutron yield Y_n ranges from 10^6 for the smallest device to 10^{11} for the PF1000.

We stress that whereas the *ID* and *SF* are practically constant at around 180 *kA/cm* and (90 *kA/cm)*/$Torr^{0.5}$ deuterium gas throughout the range of small to big devices, Y_n changes over 5 orders of magnitude.

The data of table 1 is generated from numerical experiments [5,9] and most of the data has been confirmed by actual experimental measurements and observations.

Table 2 Properties of three plasma focus devices

Plasma focus Devices	c= b/a	a (*cm*)	T_{pinch} (10^6/*K*)	v_p (*cm*/μ*s*)	r_{min} (*cm*)	z_{max} (*cm*)	Pinch Duration (*ns*)	r_{min}/a	z_{max}/a	Pinch duration/a (*ns/cm*)
PF1000	1.4	11.6	2	13	2.2	19	165	0.17	1.6	14
UNU ICTP PFF	3.4	1.0	8	26	0.13	1.4	7.3	0.14	1.4	8
PF400J	2.6	0.6	6	23	0.09	0.8	5.2	0.14	1.4	9

Table 2 compares the properties of a range of plasma focus devices. The properties being compared in this table are mainly related to the radial phase.

From table 2 we note:

i. The pinch temperature T_{pinch} is strongly correlated to the square of the radial pinch speed v_p.
ii. The radial pinch speed v_p itself is closely correlated to the value of v_a and $c=b/a$; so that for a constant v_a, v_p is almost proportional to the value of c.
iii. The dimensions and lifetime of the focus pinch scale as the anode radius 'a'.
    r_{min}/a (almost constant at 0.14-0.17)
    z_{max}/a (almost constant at 1.5)
iv. Pinch duration has a relatively narrow range of 8-14 *ns* per *cm* of anode radius.
v. The pinch duration per unit anode radius is correlated to the inverse of T_{pinch}.

T_{pinch} itself is a measure of the energy per unit mass. It is quite remarkable that this energy density at the focus pinch varies so little (factor of 5) over a range of device energy of more than 3 orders of magnitude.

This practically constant pinch energy density (per unit mass) is related to the constancy of the axial speed moderated by the effect of the values of c on the radial speed.

The constancy of r_{min}/a suggests that the devices also produce the same compression of ambient density to maximum pinch density; with the ratio (maximum pinch density)/ (ambient density) being proportional to $(a/r_{min})^2$. So for two devices of different sizes starting with the same ambient fill density, the maximum pinch density would be the same.

From the above discussion, we may put down as rule-of-thumb the following scaling relationships, subject to minor variations caused primarily by the variation in c.

i. Axial phase energy density (per unit mass) constant
ii. Radial phase energy density (per unit mass) constant
iii. Pinch radius ratio constant
iv. Pinch length ratio constant
v. Pinch duration per unit anode radius constant

1.2.2 Summarising

i. The dense hot plasma pinch of a small E_0 plasma focus and that of a big E_0 plasma focus have essentially the same energy density, and the same mass density.

ii. The big E_0 plasma focus has a bigger physical size and a bigger discharge current. The size of the plasma pinch scales proportionately to the current and to the anode radius, as does the duration of the plasma pinch.
iii. The bigger E_0, the bigger 'a', the bigger I_{peak}, the larger the plasma pinch and the longer the duration of the plasma pinch. The larger size and longer duration of the big E_0 plasma pinch are essentially the properties leading to the bigger neutron yield compared to the yield of the small E_0 plasma focus.

The above description of the plasma focus combines data from numerical experiments, consistent with laboratory observations.

The next section describes the Lee model code.

1.3 The radiative Lee model: the 5 phases

The Lee model couples the electrical circuit with plasma focus dynamics, thermodynamics, and radiation, enabling a realistic simulation of all gross focus properties. The basic model, described in 1984 [1], was successfully used to assist several projects [4-6]. Radiation-coupled dynamics was included in the five-phase code, leading to numerical experiments on radiation cooling [5]. The vital role of a finite small disturbance speed discussed by Potter in a *Z*-pinch situation [10] was incorporated together with real gas thermodynamics and radiation-yield terms. This version of the code assisted other research projects [4,8,11,12] and was web published in 2000 [13] and 2005 [14]. Plasma self-absorption was included in 2007 [13], improving the SXR yield simulation. The code has been used extensively in several machines including UNU/ICTP PFF [3,8,11,12], NX2 [12,15-17], and NX1 [15,18] and has been adapted for the Filippov-type plasma focus DENA [19]. A recent development is the inclusion of the neutron yield Y_n using a beam–target mechanism [20-24], incorporated in recent versions [5] of the code (versions later than RADPFV5.13), resulting in realistic Y_n scaling with I_{pinch} [20,21]. The versatility and utility of the model are demonstrated in its clear distinction of I_{pinch} from I_{peak} [25] and the recent uncovering of a plasma focus pinch current limitation effect [22,23], as static inductance is reduced towards zero. Extensive numerical experiments had been carried out systematically resulting in the uncovering of neutron [20,21] and SXR [26-33] scaling laws over a wider range of energies and currents than attempted before. The numerical experiments also gave insight into the nature and cause of 'neutron saturation [9,30,34]. The description, theory, code, and a broad range of results of this "Universal Plasma Focus Laboratory Facility" are available for download from [5].

A brief description of the 5-phase Lee model is given in the following.

1.3.1 The 5 phases

The five phases (*a*-*e*) are summarised [5,13,14,27, 31,33,35] as follows:

a. Axial Phase (see figure 1 left part)

Described by a snowplow model with an equation of motion which is coupled to a circuit equation. The equation of motion incorporates the axial phase model parameters: mass and current factors f_m and f_c. The mass swept-up factor f_m accounts for not only the porosity of the current sheet but also for the inclination of the moving current sheet-shock front

structure, boundary layer effects, and all other unspecified effects which have effects equivalent to increasing or reducing the amount of mass in the moving structure, during the axial phase. The current factor f_c accounts for the fraction of current effectively flowing in the moving structure (due to all effects such as current shedding at or near the back-wall, and current sheet inclination). This defines the fraction of current effectively driving the structure, during the axial phase.

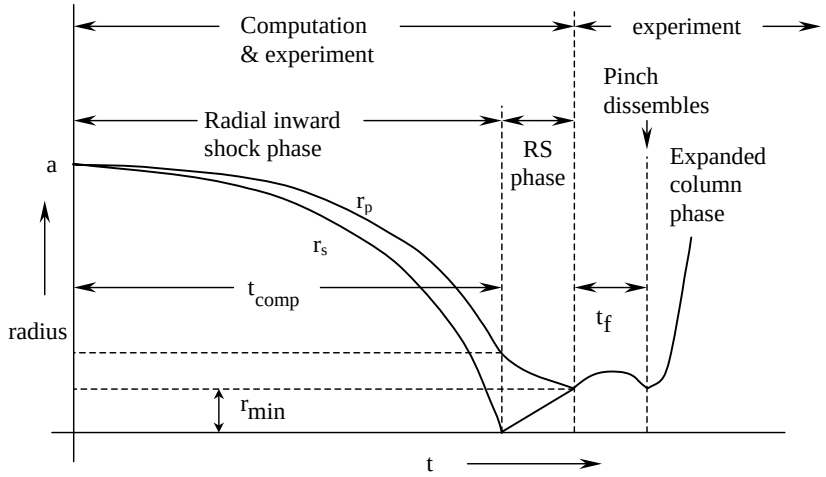

Figure 5. Schematic of radius vs time trajectories to illustrate the radial inward shock phase when r_s moves radially inwards, the reflected shock (RS) phase when the reflected shock moves radially outwards, until it hits the incoming piston r_p leading to the start of the pinch phase (t_f) and finally the expanded column phase.

b. Radial Inward Shock Phase (see figure 1 right part, also figure 2)

Described by four coupled equations using an elongating slug model. The first equation computes the radial inward shock speed from the driving magnetic pressure. The second equation computes the axial elongation speed of the column. The third equation computes the speed of the current sheath, (magnetic piston), allowing the current sheath to separate from the shock front by applying an adiabatic approximation [5,7]. The fourth is the circuit equation. Thermodynamic effects due to ionization and excitation are incorporated into these equations, these effects being particularly important for gases other than hydrogen and deuterium. Temperature and number densities are computed during this phase using shock-jump equations. A communication delay between shock front and current sheath due to the finite small disturbance speed [10,35] is crucially implemented in this phase. The model parameters, radial phase mass swept-up and current factors f_{mr} and f_{cr} are incorporated in all three radial phases. The mass swept-up factor f_{mr} accounts for all mechanisms which have effects equivalent to increasing or reducing the amount of mass in the moving slug, during the radial phase. The current factor f_{cr} accounts for the fraction of current effectively flowing in the moving piston forming the back of the slug (due to all effects). This defines the fraction of current effectively driving the radial slug.

c. Radial Reflected Shock (RS) Phase (See figure 5)

When the shock front hits the axis, because the focus plasma is collisional, a reflected shock develops which moves radially outwards, whilst the radial current sheath piston continues to move inwards. Four coupled equations are also used to describe this phase, these being for the reflected shock moving radially outwards, the piston moving radially inwards, the elongation of the annular column and the circuit. The same model parameters f_{mr} and f_{cr} are

used as in the previous radial phase. The plasma temperature behind the reflected shock undergoes a jump by a factor close to 2. Number densities are also computed using the reflected shock jump equations.

d. Slow Compression (Quiescent) or Pinch Phase (See figure 5)

When the out-going reflected shock hits the inward moving piston, the compression enters a radiative phase in which for gases such as neon, radiation emission may actually enhance the compression where we have included energy loss/gain terms from Joule heating and radiation losses into the piston equation of motion. Three coupled equations describe this phase; these being the piston radial motion equation, the pinch column elongation equation and the circuit equation, incorporating the same model parameters as in the previous two phases. The duration of this slow compression phase is set as the time of transit of small disturbances across the pinched plasma column. The computation of this phase is terminated at the end of this duration.

e. Expanded Column Phase

To simulate the current trace beyond this point we allow the column to suddenly attain the radius of the anode, and use the expanded column inductance for further integration. In this final phase the snow plow model is used, and two coupled equations are used similar to the axial phase above. This phase is not considered important as it occurs after the focus pinch.

We note [31] that in radial phases *b, c* and *d,* axial acceleration and ejection of mass caused by necking curvatures of the pinching current sheath result in time-dependent strongly center-peaked density distributions. Moreover the transition from phase *d* to phase *e* is observed in laboratory measurements to occur in an extremely short time with plasma/current disruptions resulting in localized regions of high densities and temperatures. These centre-peaking density effects and localized regions are not modeled in the code, which consequently computes only an average uniform density, and an average uniform temperature which are considerably lower than measured peak density and temperature. However, because the four model parameters are obtained by fitting the computed total current waveform to the measured total current waveform, the model incorporates the energy and mass balances equivalent, at least in the gross sense, to all the processes which are not even specifically modeled. Hence the computed gross features such as speeds and trajectories and integrated soft x-ray yields have been extensively tested in numerical experiments for several machines and are found to be comparable with measured values.

1.4 Using the Lee model as reference for diagnostics

1.4.1 From measured current waveform to modelling for diagnostics

The Lee model code [5,13,14] is configured [9] to work as any plasma focus by inputting:

Bank parameters, L_0, C_0 and stray circuit resistance r_0;
Tube parameters b, a and z_0;
Operational parameters V_0 and P_0 and the fill gas.

The computed total current waveform is fitted to the measured waveform by varying model parameters f_m, f_c, f_{mr} and f_{cr} one by one, until the computed waveform agrees with the measured waveform.
First, the axial model factors f_m, f_c are adjusted (fitted) until the features in figure 6: **'1'** computed rising slope of the total current trace; **'2'** the rounding off of the peak current as well as **'3'** the peak current itself are in reasonable (typically very good) fit with the measured total current trace (see figure 6, measured trace fitted with computed trace).

Then we proceed to adjust (fit) the radial phase model factors f_{mr} and f_{cr} until features **'4'** the computed slope and **'5'** the depth of the dip agree with the measured values. Note that the fitting of the computed trace with the measured current trace is done up to the end of the radial phase which is typically at the bottom of the current dip. Fitting of the computed and measured current traces beyond this point is not done. If there is significant divergence of the computed with the measured trace beyond the end of the radial phase, this divergence is not considered important.

In this case, after fitting the five features **'1'** to **'5'** above, the following fitted model parameters are obtained: f_m=0.1, f_c=0.7, f_{mr}=0.12, f_{cr}=0.68.

From experience it is known that the current trace of the focus is one of the best indicators of gross performance. The axial and radial phase dynamics and the crucial energy transfer into the focus pinch are among the important information that is quickly apparent from the current trace [27-29].

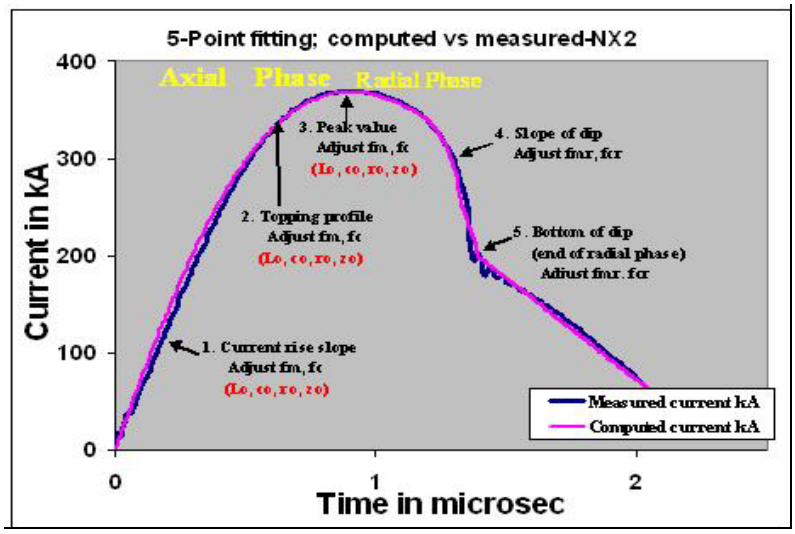

Figure 6. The 5-point fitting of computed current trace to measured (reference) current trace. **Point 1** is the current rise slope. **Point 2** is the topping profile. **Point 3** is the peak value of the current. **Point 4** is the slope of the current dip. **Point 5** is the bottom of the current dip. Fitting is done up to point 5 only. Further agreement or divergence of the computed trace with/from the measured trace is only incidental and not considered to be important.

The exact time profile of the total current trace is governed by the bank parameters, by the focus tube geometry and the operational parameters. It also depends on the fraction of mass swept-up and the fraction of sheath current and the variation of these fractions through the axial and radial phases. These parameters determine the axial and radial dynamics,

specifically the axial and radial speeds which in turn affect the profile and magnitudes of the discharge current.

There are many underlying mechanisms in the axial phase such as shock front and current sheet structure, porosity and inclination, boundary layer effects and current shunting and fragmenting which are not simply modeled; likewise in the radial phase mechanisms such as current sheet curvatures and necking leading to axial acceleration and ejection of mass, and plasma/current disruptions. These effects may give rise to localized regions of high density and temperatures. The detailed profile of the discharge current is influenced by these effects and during the pinch phase also reflects the Joule heating and radiative yields. At the end of the pinch phase the total current profile also reflects the sudden transition of the current flow from a constricted pinch to a large column flow. Thus the discharge current powers all dynamic, electrodynamic, thermodynamic and radiation processes in the various phases of the plasma focus. Conversely all the dynamic, electrodynamic, thermodynamic and radiation processes in the various phases of the plasma focus affect the discharge current. It is then no exaggeration to say that the discharge current waveform contains information on all the dynamic, electrodynamic, thermodynamic and radiation processes that occur in the various phases of the plasma focus. This explains the importance attached to matching the computed total current trace to the measured total current trace in the procedure adopted by the Lee model code. Once matched, the fitted model parameters assure that the computation proceeds with all physical mechanisms accounted for, at least in the gross energy and mass balance sense.

1.4.2 Diagnostics-time histories of dynamics, energies and plasma properties computed from the measured total current waveform by the code

During every adjustment of each of the model parameters the code goes through the whole cycle of computation. In the last adjustment, when the computed total current trace is judged to be reasonably well fitted in all 5 waveform features, computed time histories are presented, in figure 7a-7o as an example, as follows: for the NX2 operated at 11 *kV*, 2.6 *Torr* neon [9,33].

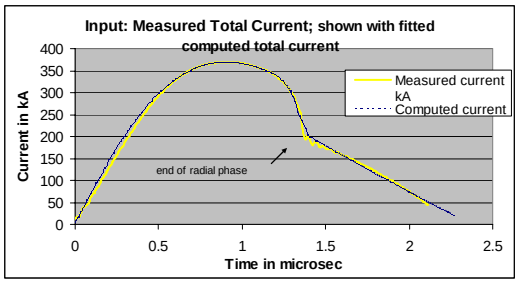

Figure 7a. Fitted computed I_{total}

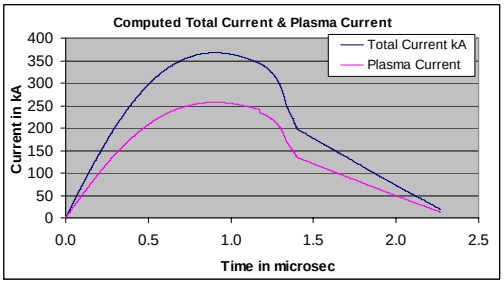

Figure 7b. Computed I_{total} & I_{plasma}

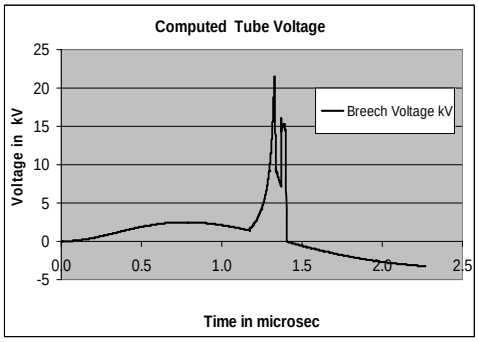

Figure 7c. Tube voltage

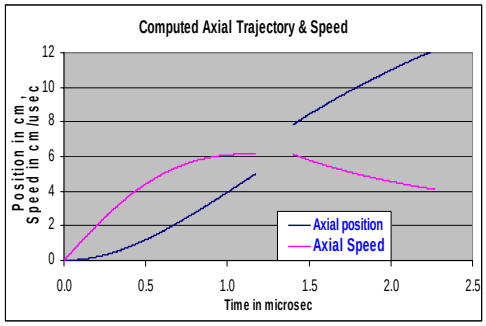

Figure 7d. Axial trajectory and speed

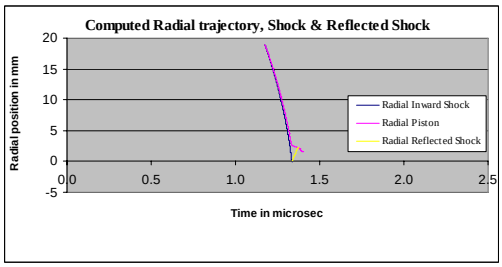

Figure 7e. Radial trajectories

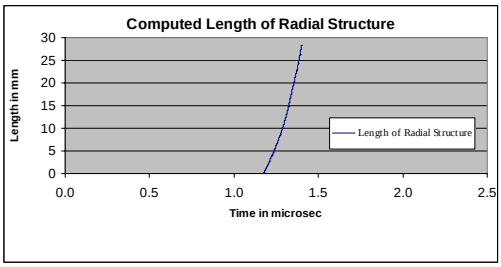

Figure 7f. Length of elongating structure

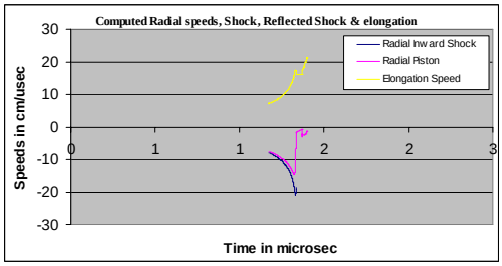

Figure 7g. Speeds in radial phases

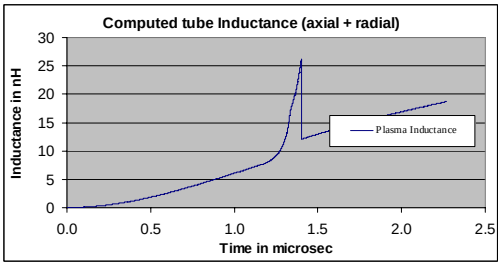

Figure 7h. Tube inductance-axial & radial phases

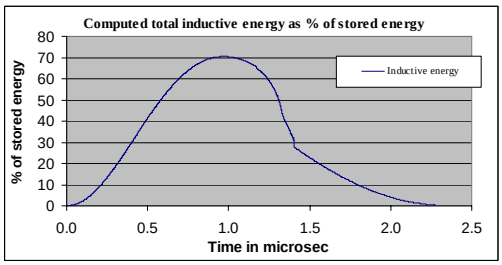

Figure 7i. Total inductive energy

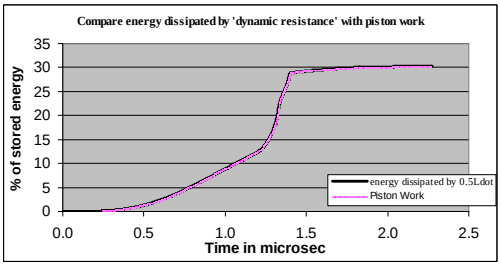

Figure 7j. Piston work and DR energy; both traces overlap

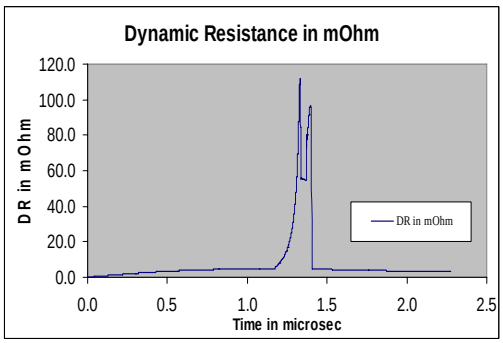

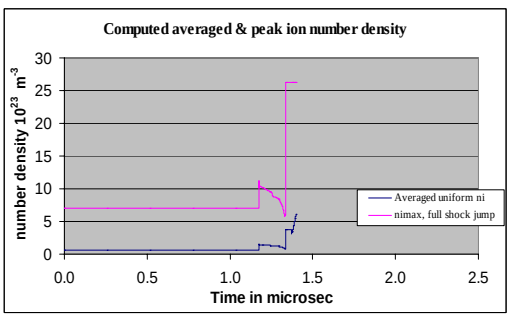

Figure 7k. DR axial and radial phases

Figure 7l. Peak & averaged uniform n_i

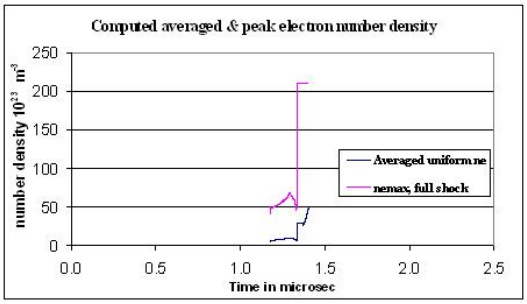

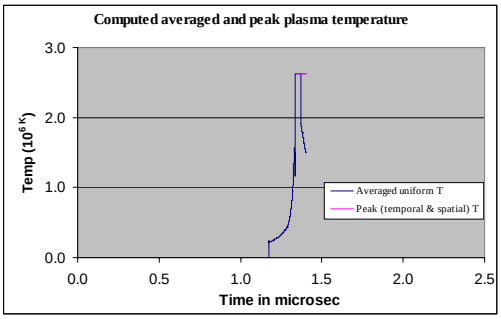

Figure 7m. Peak & averaged uniform n_e

Figure 7n.Peak and averaged uniform T

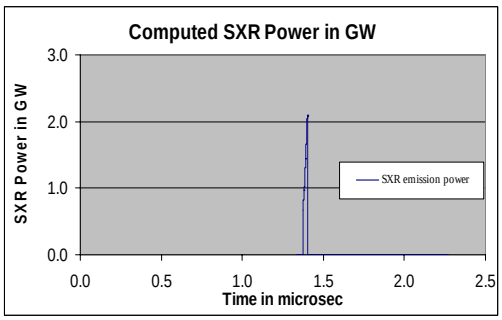

Figure 7o. Neon Soft x-ray power

1.4.3 Comments on computed quantities by Lee model code

i. The computed total current trace typically agrees very well with the measured because of the fitting. The end of the radial phase is indicated in Figure 7a. Plasma currents are rarely measured. We had done a comparison of the computed plasma current with measured plasma current for the Stuttgart PF78 which shows good agreement of our computed to the measured plasma current [28]. The computed plasma current in this case of the NX2 is shown in figure 7b.

ii. The computed tube voltage is difficult to compare with measured tube voltages in terms of peak values, typically because of poor response time of voltage dividers. However the computed waveform shape in figure 7c is general as expected.

iii. The computed axial trajectory and speed, agree with experimental obtained time histories. Moreover, the behaviour with pressure, running the code at different pressures, agrees well with experimental results. The radial trajectories and speeds are difficult to measure. The computed trajectories figure 7e agrees with the scant experimental data available. The length of the radial structure is shown in figure 7f. Computed speeds radial shock front and piston speeds and speed of the elongation of the structure are shown in figure 7g.

iv. The computed inductance (figure 7h) shows a steady increase of inductance in the axial phase, followed by a sharp increase (rising by more than a factor of 2 in a radial phase time interval about 1/10 the duration of the axial phase for the NX2).

v. The inductive energy ($0.5LI^2$) peaks at 70% of initial stored energy, and then drops to 30% during the radial phase, as the sharp drop of current more than offsets the effect of sharply increased inductance (figure 7i).

vi. In figure 7j is shown the work done by the magnetic piston, computed using force integrated over distance method. Also shown is the work dissipated by the dynamic resistance, computed using dynamic resistance power integrated over time. We see that the two quantities and profiles agree exactly. This validates the concept of half *Ldot* as a dynamic resistance.

vii. Dynamic resistance, DR (DR will be discussed in Module 2, Section 2.3; Note 2). The piston work deposited in the plasma increases steadily to some 12% at the end of the axial phase and then rises sharply to just below 30% in the radial phase. Dynamic resistance is shown in figure 7k. The values of the DR in the axial phase, together with the bank surge impedance, are the quantities that determine I_{peak}.

viii. The ion number density has a maximum value derived from shock-jump considerations, and an averaged uniform value derived from overall energy and mass balance considerations. The time profiles of these are shown in the figure 7l. The electron number density (figure 7m) has similar profiles to the ion density profile, but is modified by the effective charge numbers due to ionization stages reached by the ions.

ix. Plasma temperature too has a maximum value and an averaged uniform value derived in the same manner; are shown in figure 7n. Computed neon soft x-ray power profile is shown in figure 7o. The area of the curve is the soft x-ray yield in *J*. Pinch dimensions and lifetime may be estimated from figures 7e and 7f.

x. The model also computes the neutron yield, for operation in deuterium, using a phenomenological beam-target mechanism [25-27]. The model does not compute a time history of the neutron emission, only a yield number Y_n.

Thus as is demonstrated above, the model code when properly fitted is able to realistically model any plasma focus and act as a guide to diagnostics of plasma dynamics, trajectories, energy distribution and gross plasma properties.

1.4.4 Scaling parameters of the plasma focus pinch

The gross dynamics of the plasma focus is discussed in terms of phases. The dynamics of the axial and radial phases is computed using respectively a snowplow and an elongating slug model. A reflected shock phase follows, giving the maximum compression configuration of the plasma focus pinch. An expanded column phase is used to complete the post-focus electric current computation. Parameters of the gross focus pinch obtained from the computation, supplemented by experiments may also be summarised as follows:

Table 3

Plasma Focus Pinch Parameters		**Deuterium**	**Neon (for SXR)**
minimum radius	r_{min}	$0.15a$	$0.05a$
max length (hollow anode)	z	1.5a	$1.6a$
radial shock transit	t_{comp}	$5\text{x}10^{-6}a$	$4\text{x}10^{-6}a$
pinch lifetime	t_p	$10^{-6}a$	$10^{-6}a$

where, for the times in *s*, the value of anode radius, *a*, is in *m*. For the neon calculations radiative terms are included; and the stronger compression (smaller radius) is due to thermodynamic effects.

1.5 Insights on plasma focus from numerical experiments using Lee model code

Using the Lee model code, series of experiments have been systematically carried out to look for behaviour patterns of the plasma focus.

Insights uncovered by the series of experiments include:

i. pinch current limitation effect as static inductance is reduced;
ii. neutron and SXR scaling laws;
iii. a global scaling law for neutrons versus storage energy combining experimental and numerical experimental data; and
iv. the nature and a fundamental cause of neutron saturation.

These significant achievements are accomplished within a period of twenty months of intensive numerical experimentation in 2008 to 2009. The numerical experimental research continues in 2010 with widening international collaboration.

References

[1] Lee, S. Plasma focus model yielding trajectory and structure. In *Radiations in Plasmas*, McNamara, B., Ed.; World Scientific, Singapore: **1984**; Volume II, pp. 978–987.
[2] Glenn Millam Focus Fusion Society
[3] Muhammad Shahid Rafique. PhD thesis (in preparation) NTU, Singapore.
[4] S.Lee, S.P.Moo, C.S.Wong, A.C.Chew. Twelve Years of UNU/ICTP PFF- A Review. IC/98/231, ICTP Preprint, International Centre for Theoretical Physics, Trieste, Italy (1998), 101 pages.
[5] Lee S Radiative Dense Plasma Focus Computation Package: RADPF
http://www.intimal.edu.my/school/fas/UFLF/File1RADPF.htm
http://www.plasmafocus.net/IPFS/modelpackage/File1RADPF.htm
[6] S.Lee, T.Y.Tou, S.P.Moo, M.A.Eissa, A.V.Gholap, K.H.Kwek, S.Mulyodrono, A.J. Smith, Suryadi, W.Usala, M. Zakaullah. A simple facility for the teaching of plasma dynamics and plasma nuclear fusion. Amer J. Phys., USA, **1988**, 56: 62-68.
[7] http://www.intimal.edu.my/school/fas/UFLF/
[8] S Lee and A Serban A, "Dimensions and lifetime of the plasma focus pinch," IEEE Trans. Plasma Sci., 24, no.3, **1996**, 1101-1105.
[9] Lee S. Diagnostics and Insights from Current waveform and Modelling of Plasma Focus. Keynote address: IWPDA, Singapore 2-July **2009**
[10] Potter, D. E. The formation of high-density z-pinches. *Nucl. Fusion.* **1978,** *18*, 813–823.
[11] M.H.Liu. Soft X-Rays from Compact Plasma Focus. PhD thesis. NTU, Singapore, **1997**
[12] S.Lee, P.Lee, G.Zhang, X. Feng, V.Gribkov, M.Liu, A.Serban & T.K.S. Wong. High Repetition High Performance Plasma Focus as a Powerful Radiation Source- IEEE Trans Plasma Science 26(4) 1119-1126 (**1998**).
[13] S. Lee, **2000–2007**. [Online]. Available: http://ckplee.myplace.nie.edu.sg/ plasmaphysics/
[14] S. Lee, *ICTP Open Access Archive*, **2005**. [Online]. Available: http://eprints.ictp.it/85/
[15] G.X.Zhang. Plasma Soft x-ray source for Microelectronics lithography. PhD thesis, NTU, Singapore **1999**.
[16] S.Lee, V.Kudryashov, P.Lee, G.Zhang, A..Serban, X..Feng, M.Liu, and T.K.S.Wong. Lithography Using a Powerful Plasma Focus Soft X-ray Source. International Congress on Plasma Physics, Prague, Czech Republic, June **1998**. To be published in Procs.

[17] D Wong, P Lee, T Zhang, A Patran, T L Tan, R S Rawat and S Lee, "An improved radiative plasma focus model calibrated for neon-filled NX2 using a tapered anode," Plasma Sources Sci. Technol. 16, **2007**, pp. 116-123.

[18] E P Bogolyubov, V D Bochkov, V A Veretennikov, L T Vekhoreva, V A Gribkov, A V Dubrovskii, Yu P Ivanov, A I Isakov, O N Krokhin, P Lee, S Lee, V Ya Nikulin, A Serban, P V Silin, X Feng and G X Zhang, "A powerful soft x-ray source for x-ray lithography based on plasma focusing" 1998 *Phys. Scripta.*, vol. 57, **1998**, pp. 488-494.

[19] V Siahpoush, M A Tafreshi, S Sobhanian and S Khorram, "Adaptation of Sing Lee's model to the Filippov type plasma focus geometry," Plasma Phys. Control. Fusion 47, **2005**, pp. 1065-1072.

[20] S. Lee and S.H. Saw "Neutron scaling laws from numerical experiments," *J. Fusion Energy*, **2008**, *27*, no. 4, pp. 292–295.

[21] S. Lee S. "Current and neutron scaling for megajoule plasma focus machines," *Plasma Phys. Control. Fusion*, **2008**, *50*, no. 10, p. 105 005 (14pp).

[22] S. Lee and S.H. Saw "Pinch current limitation effect in plasma focus," *Appl. Phys. Lett.*, **2008**, *92*, no. 2, p. 021 503.

[23] S. Lee S, P. Lee, S H. Saw and R.S. Rawat, "Numerical experiments on plasma focus pinch current limitation," *Plasma Phys. Control. Fusion*, **2008**, *50*, no. 6, 065 012 (8pp).

[24] V. A. Gribkov, A. Banaszak, S. Bienkowska, A.V. Dubrovsky, I. Ivanova-Stanik, L. Jakubowski, L. Karpinski, R.A. Miklaszewski, M. Paduch, M.J. Sadowski, M. Scholz, A. Szydlowski and K. Tomaszewski "Plasma dynamics in the PF-1000 device under fullscale energy storage: II. Fast electron and ion characteristics versus neutron emission parameters and gun optimization perspectives," *J. Phys. D,Appl. Phys.*, **2007**, *40*, no. 12, 3592–3607

[25] S Lee, S H Saw, P C K Lee, R S Rawat and H Schmidt, "Computing plasma focus pinch current from total current measurement," Appl. Phys. Lett. 92 , **2008**, 111501

[26] Akel M., Al-Hawat Sh., Lee S. "Pinch Current and Soft x-ray yield limitation by numerical experiments on Nitrogen Plasma Focus". *J Fusion Energy* DOI 10.1007/s10894-009-9238-6. First online 21 August **2009**

[27] Saw S. H., Lee P. C. K., Rawat R. S. & Lee S. 2009 'Optimizing UNU/ICTP PFF Plasma Focus for Neon Soft X-ray Operation' *IEEE Trans on Plasma Sc*, **2009**, *37*, 1276-1282.

[28] Saw S. H. and Lee S. " Scaling laws for plasma focus machines from numerical experiments". Invited paper: IWPDA, Singapore 2&3 July **2009**

[29] Saw S. H. and Lee S. "Scaling the plasma focus for fusion energy considerations". Tubav Conferences: Nuclear & Renewable Energy Sources, Ankara, Turkey, 28 & 29 September **2009**.

[30] Lee S."Nuclear fusion and the Plasma Focus", Invited paper Tubav Conferences: Nuclear & Renewable Energy Sources Ankara, Turkey, 28 & 29 September **2009**.

[31] Lee S., Saw S. H., Lee P. & Rawat R. S., "Numerical Experiments on Neon plasma focus soft x-rays scaling", *Plasma Physics and Controlled Fusion*, **2009**, *51*, 105013 (8pp).

[32] Akel M., Al-Hawat Sh., Lee S. "Numerical Experiments on Soft X-ray Emission Optimization of Nitrogen Plasma in 3 kJ Plasma Focus SY-1 Using Modified Lee Model", *J Fusion Energy* DOI 10.1007/s10894-009-9203-4 First online, May 19, **2009.**

[33] Lee S., Rawat R. S., Lee P., S H Saw S. H., Soft x-ray yield from NX2 plasma focus, *JOURNAL OF APPLIED PHYSICS*, **2009,** *106*, 023309.

[34] Lee S. "Neutron Yield Saturation in Plasma Focus-A fundamental cause" *APPLIED PHYSICS LETTERS*, **2009**, *95*, 151503 published online 15 October 2009

[35] Lee S., Saw S. H., Soto L., Moo S. P., Springham S. V., Numerical experiments on plasma focus neutron yield versus pressure compared with laboratory experiments, *Plasma Phys. Control. Fusion*, **2009,** *51* 075006

[36] Lee, S (**2004**) *Characterising the Plasma Focus Pinch and Speed Enhancing the Neutron Yield.* In: First Cairo Conference on Plasma Physics & Applications. International Cooperation Bilateral Seminars (Vol 34). Forschungszentrum Juelich GmbH, Juelich, Germany, pp. 27-33. ISBN 3-89336-374-2 http://eprints.ictp.it/39/

Module 2: Universal Plasma Focus Laboratory-The Lee model code

Follow the instructions (written for EXCEL 2007 but easily adapted to EXCEL 2003) in the following notes. You may also wish to refer to the supplementary notes **SP1.doc** (scroll down to pg 77, after Module 7)**.** Instructions are given in some details in order to accommodate participants who may not be familiar with EXCEL. Those who find the instructions unnecessarily detailed may wish to skip the unnecessary lines. The code seems to be unnecessarily cumbersome when used with EXCEL 2007. So EXCEL 2003 is preferred.

Summary

The material

You should have **RADPFV5.15de.xls (contained in the e-folder "Code and Data" accompanying this file)** on your Desktop for the next step. Please also ensure you have kept an identical original copy in a RESERVE folder. You are going to work with the desktop copy; and may be altering it. Each time you need an unaltered copy; you may copy from the reserve folder and paste it onto the desktop.

2.1 Introduction to the Worksheet

2.1.1 Opening the worksheet

(*Note: Click means the ordinary click on the left button of the mouse; as distinct from the term Right Click, which means the special click on the right button of the mouse.*)

Double click on **RADPFV5.15de.xls**
Work sheet appears and should look like Figure 1 [shown only as an example]; for the following please refer not to Figure 1 but to your worksheet.

Security pop-up screen appears.
Click on **enable macros**
The Active Sheet opens and is ready for use.

[EXCEL 2007: Security Warning "Macros have been disabled" appears at top left hand corner of Worksheet with side box "options".
Click on "options"- select the button "Enable this content"- click OK
After this procedure, the worksheet is macro-enabled and is ready for firing.]

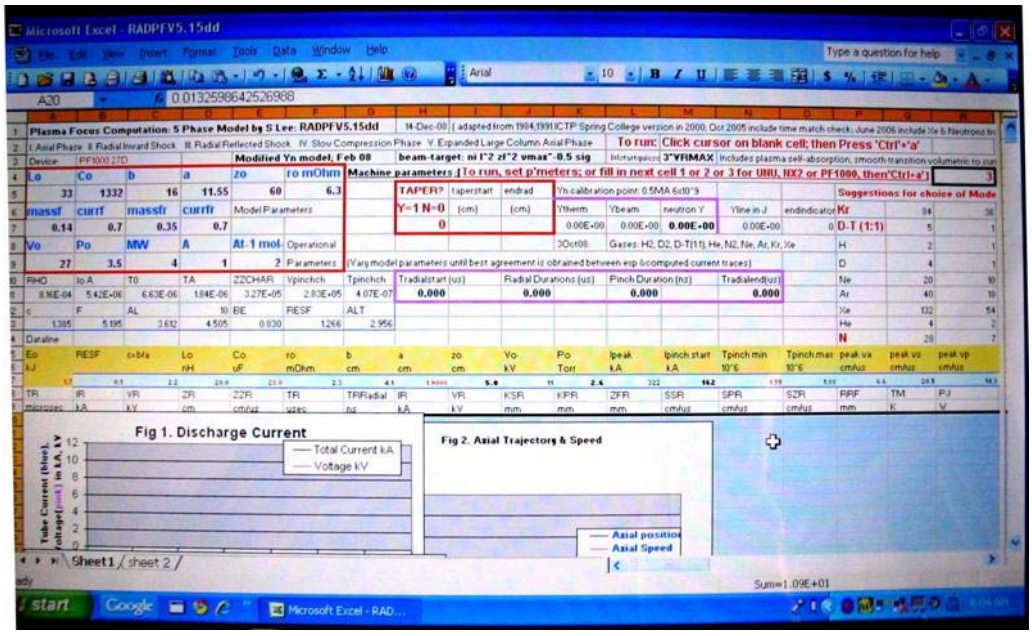

Figure 1. Appearance of worksheet-EXCEL 2003 version; EXCEL 2007 version should not look too different.

2.1.2 Preliminary orientation for setting controls

(For the following instructions, use your Excel Sheet; not the above image)

Device configuration:
(*Note: Each Cell of the Excel Worksheet is defined by a Column alphabet A, B, or C….. and a Row number 1, 2 or 3 etc. The Column alphabets are shown along the top border of the worksheet. The Row numbers are shown along the left border of the Worksheet. For example, Cell A4 is located at column A row 4. Another example: A4-F9 refers to the block of cells within the rectangle bordered by row A4-F4, column A4-A9, row A9-F9 and column*

F4-F9; the larger orange-red bordered rectangle, containing 6x6 cells, near the top left of figure1.)

Locate Cells A4 to F9. These cells are for setting bank parameters, tube parameters, operating parameters and model parameters.

Taper: Control Cells for anode taper are normally inactivated by typing 0 (number zero) in Cell H7. **Ensure that H7 is filled with 0** (number zero); unless anode taper feature is needed.
One Click Device: This control cell R4 allows choice of a specific plasma focus using numbers; currently 3 machines are available chosen with numbers 1, 2 or 3. **Ensure that R4 is filled with the number 0. (**Otherwise the code will keep defaulting to the selected machine '1' or '2' or '3'.)

2.1.3 Preliminary orientation for computed results

Cells A10-G13: computed characteristic quantities of the configured plasma focus.
Cells K6-M7: computed neutron yield, component & total; if operated in deuterium
Cell N6-N7: computed SXR line radiation
Cells H10-N11: computed durations of axial phase, radial phase and pinch phase and end time of radial phase.

Cells A15-AI17: dataline: contains data on row 17 with corresponding labels (and units) in rows 15 and 16. Data: E_0, RESF, $c=b/a$, L_0, C_0, r_0, b, a, z_0, V_0, P_0, I_{peak}, $I_{pinchstart}$, $T_{pinchmin}$, $T_{pinchmax}$, peak v_a, peak v_s, peak v_p, a_{min} (which is r_{min}), z_{max}, pinch duration, V_{max}, $n_{ipinchmax}$, Y_n, *Qsxr*, *Qsxr%*, f_m, f_c, f_{mr}, f_{cr}, *EINP*, *taxialend*, *SF*, *ID* and Q_{line}; others may be added from time to time.

This is a recently introduced very useful feature; enables computed data for each shot to be copied and pasted onto another sheet; so different shots may be placed in sequence, and comparative charts may be made.

Columns A20 to AP20: computed point by point results (data are correspondingly labeled in row A18 with units in row 19) for the following quantities respectively:

Time in μs, total current, tube voltage, axial position, axial speed, time of radial phase in μs measured from the start of axial phase, time of radial phase in *ns* from the start of the radial phase, corresponding quantities of current, voltage, radial shock position, radial piston position, radial pinch length, radial shock, piston and pinch elongation speeds, reflected shock position, plasma temperature, Joule power, Bremsstrahlung, recombination, line emission powers, total radiation power, total power, Joule, Bremsstrahlung, recombintion, line emission energies, total radiation energy, total energy, plasma self-absorption correction factor, black-body power, specific heat ratio and effective charge number, number thermonuclear neutrons, number beam target neutrons, number total neutrons, ion density, volume radiation power, surface radiation power, plasma self-absorption correction factor , radial phase piston work in % of E_0, neon SXR energy emission.

Each computed quantity as a function of time (displayed in the relevant column) is displayed in a column. After a run each of these columns is typically filled to several thousand cells.

Computed results are also summarized in 8 figures:

Figure 1: (Top left) total discharge current and tube voltage
Figure 2: (Top right) axial trajectory and speed
Figure 3: radial trajectories
Figure 4: total tube voltage during radial phase
Figure 5: radial speeds
Figure 6: plasma temperature
Figure 7: Joule heat and radiation energies
Figure 8: Joule power and radiation powers

An additional figure 8a on the right displays the specific heat ratio and effective charge number during the radial phase.

2.2 Configuring the Universal Plasma Focus Laboratory (UPFL)

2.2.1 Configuring the worksheet for a specific machine

As a first exercise we configure the UPFL so it operates as the NX2, the High-repetition rate neon focus developed for SXR lithography in Singapore.

The parameters are:

Bank: L_0=20 *nH*, C_0=28 μF, r_0=2.3 $m\Omega$
Tube: b=4.1 *cm*, a=1.9 *cm*, z_0=5 *cm*
Operation: V_0=11 *kV*, P_0=2.63 *Torr*, *MW*=20, *A*=10, *At-Mol*=1 (these last 3 defines neon for the code i.e. molecular (atomic) weight, atomic number and whether atomic or molecular)

Model: massf (f_m)=0.0635, currf (f_c)=0.7, massfr (f_{mr}) =0.16, currfr (f_{cr})=0.7; these are the mass and current factors for the axial and radial phases.
(Note: 1. *These model parameters had been fitted earlier by us so that the computed total current best fits a measured total current trace from the NX2.*
Note:2. *We will carry out exercises in fitting model parameters in Module 3*)

Configuring: Key in the following: (e.g. in Cell A5 key in 20 [for 20nH], Cell B5 key in 28 [for 28μF] etc.

	A5	B5	C5	D5	E5	F5
	20	28	4.1	1.9	5	2.3
Then	A9	B9	C9	D9	E9	
	11	2.63	20	10	1	
Then	A7	B7	C7	D7		
	0.0635	0.7	0.16	0.7		

You may of course find it easier to follow the labels in A4-F4, to key in A5-F5 for the relevant parameters; i.e. A4 states L_0 *nH*; so fill in below it in A5 20 ; and so on.
For identification purposes key in at B3 'NX2'

2.3 Firing a shot in NX2

Place the cursor in any blank non-active space, e.g. G8. (point the cursor at G8 and **click** the mouse). Press 'Ctrl' and 'A' (equivalent to firing a shot).

The programme runs and in less than a minute the run has completed and your worksheet will look something like figure 2 below:

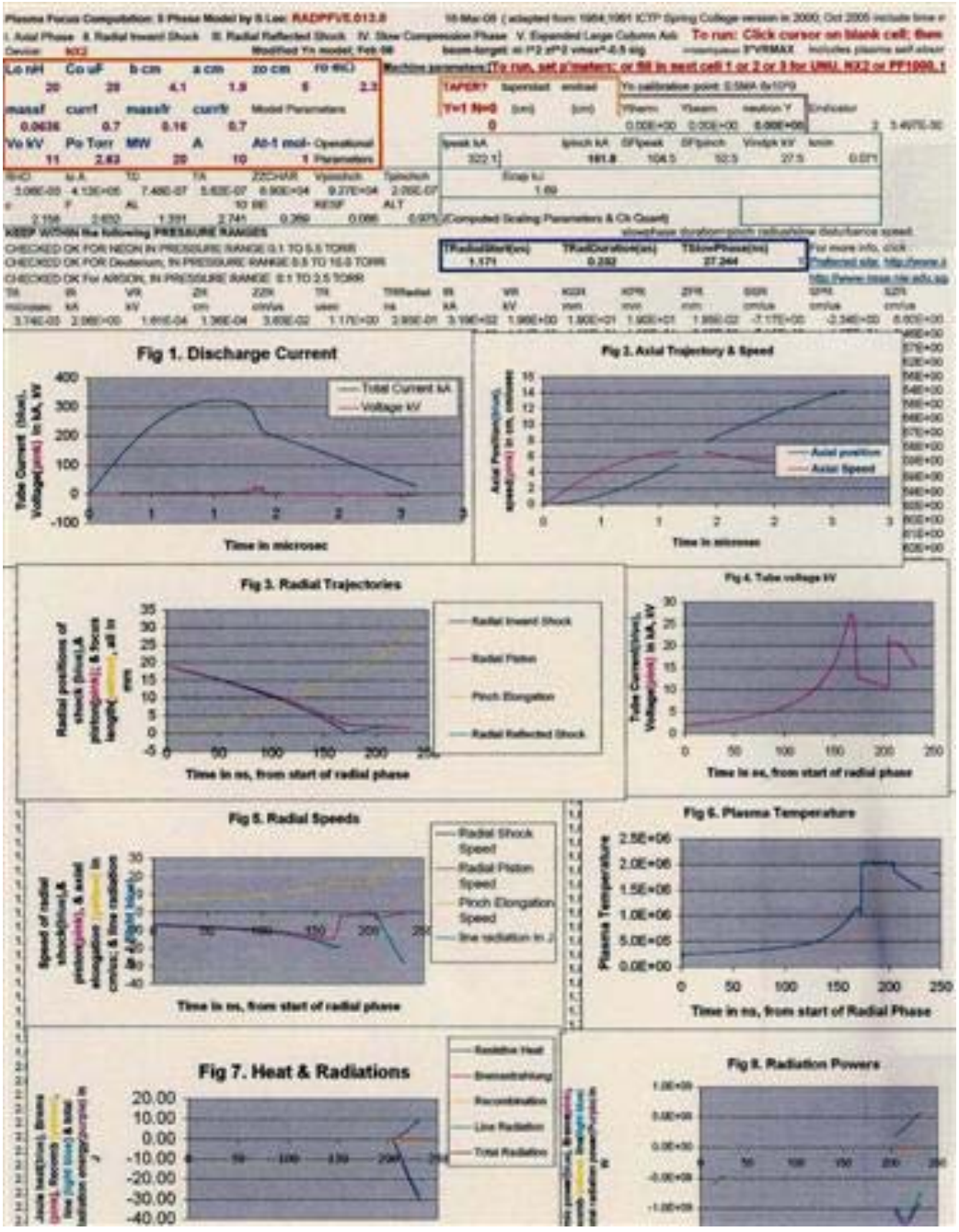

Figure 2. Appearance of Worksheet after a shot.

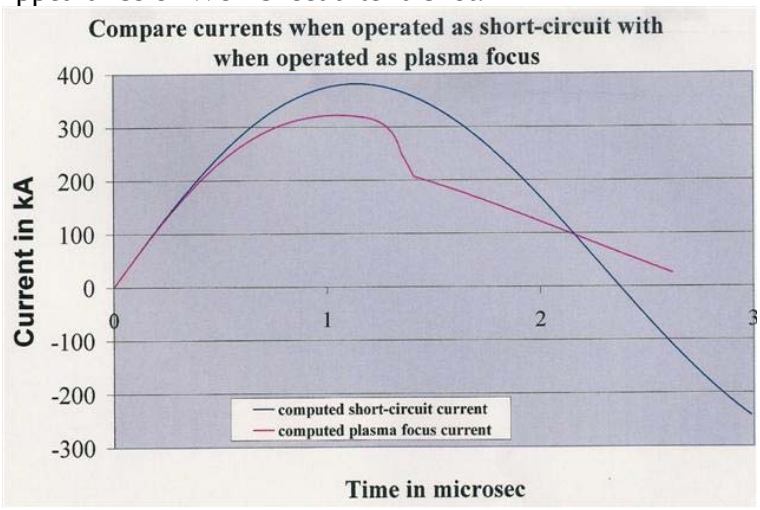

Figure 3. Plasma focus current is distorted from unloaded current waveform.

In figure 3 is superimposed a current waveform (in blue; *you do not have this waveform*) of the plasma focus short-circuited across its input end insulator; with the current waveform (pink) you have just computed [see your worksheet figure 2] (*In a later session you will learn how to do the short-circuit computation and superimposition*).

Notes:

Note 1
The first important point to stress (and one that should never be forgotten) is that the plasma focus current waveform is very much distorted from the damped sinusoid of the *L-C-R* discharge without the plasma focus load (figure 3). The 'distortions' are due to the electrodynamical effects of the plasma motion, including the axial and radial dynamics and the emission of SXR from the Neon plasma. The way we use the code is based on the premise that the features of these 'distortions' contain the information of the plasma electrodynamics.

The plasma focus loads the electrical circuit in the same manner as an electric motor loads its driving circuit. The loading may be expressed as a resistance. More specifically we may compute the loading or 'dynamic' resistance as follows in Note 2; which shows that the dynamic resistance due to the motion in the axial phase is more than the stray resistance of the capacitor bank in the case of the NX2. Note 3 shows further that the dynamic resistance due to the plasma motion in the radial phase is so large as to completely dominate the situation. This causes the large current dip as shown in figure 3.

Note 2

As an example we may estimate the effect of one of the electrodynamical effects. The quantity $(1/2)(dL/dt)$ is a dynamic resistance.

In the axial phase $L=(\mu/2\pi)*ln(b/a)*z$ where μ is permeability and z is the position of the current sheath.

Differentiating, $0.5*dL/dt = 10^{-7} * ln(4.1/1.9)$*axial speed~0.8 $m\Omega$ per 10^4 *m/s* axial speed; or 0.8 $m\Omega$ per unit speed of *cm/μs*. At the peak axial speed of 6.6 *cm/μs* (see figure 2 of worksheet), that gives us a circuit loading of ~ 5 $m\Omega$; which is reduced to 3.5 $m\Omega$ when we consider the effect of the current factor. This is more than the loading of the stray resistance r_o of 2.3 $m\Omega$. So the axial motion of the current sheath is an important loading to the circuit.

Note 3

Continuing along this vein we may estimate the dynamic resistive loading of the current sheath motion in the radial phase when $L = (\mu/2\pi)*\ln(b/r_p)*z_f$, where r_p= radial piston position and z_f = length of the elongating column; both r_p & z_f changing with time.

Thus $dL/dt = (\mu/2\pi)*\ln(b/r_p)*dz_f/dt + (\mu/2\pi)*z_f*(dr_p/dt)/r_p$

$= 2*10^{-7}*\left(ln(b/r_p)*dz_f/dt + z_f*(dr_p/dt)/r_p\right)$ [both terms RHS are positive]

In the section (2.4) below we will get from the output figures of the worksheet the following values at around the time of peak piston speed:

r_p~2.4 *mm*, z_f~15 *mm*, dr_p/dt~13.5 *cm/μs* [$1.35*10^5$ *m/s*]; dz_f/dt~$1.7*10^5$ *m/s*; Substituting into expression above, we get at the time of peak piston speed dL/dt~190 $m\Omega$; giving us (after considering current factor of 0.7) still around 130 $m\Omega$ of dynamic resistive loading due to the current sheath motion. This dynamic resistance (compared to r_0 of just 2.3 $m\Omega$) dominates the current profile at this stage.

Note 4

$d[LI]/dt$ generates an induced voltage; with one important component in this situation being $I*(dL/dt)$. Since we have already estimated that dL/dt~0.19 Ω; multiplying this by 0.7x200 *kA* of current (which is the approx value of current at this time) gives us just under 30 *kV*. So we note that the dynamics at this time (just as the radial shock is going on axis) contributes a back voltage of ~30 *kV* through this term.

The other term $L*(dI/dt)$ terms is negative; so the maximum induced voltage is considerably less than 30 *kV*, as you can see from figure 2.

Note 5

As a separate exercise which you may like to do one day: What is the basis for saying that $(1/2)*(dL/dt)$ is a dynamic resistance? Can you show this by examining the power term in the situation when an inductance is changing? Compare the inductive power flow: $(d/dt)(0.5*L*I^2)$ and the total power flow: $VI=I*(d/dt)(L*I)$.

What do you notice?

2.4 Studying the results

(The results are obtained from your **Excel Sheet**; not from the above images in figure 2) Remember we are operating a neon plasma focus.

Here are some important quantities obtained from the data line in row 17.

Computed	I_{peak}:	L17	322 *kA*
	I_{pinch}:	M17	162 *kA* (pinch current at start of pinch phase)
	Peak tube voltage:	V17	26.1 *kV*
	k_{min}:	S17	0.075 (r_{min} or a_{min}/a) [you may also check this against figure 3 of the worksheet.]

Durations: H11-N11

Axial phase ends at 1.172 μ*s*

Radial phase ends at 1.407 μ*s* (add 1.172 to 0.235 μs) of which the last 26.2 *ns* is the pinch phase.

Now we study the **various figures displayed on the worksheet**, Sheet1 (also shown in figure 2).

Fig 1

Computed current trace; One point of interest is to locate the ends of axial and radial phases on this trace; as well as the start and end of the pinch phase. To do this, select Fig 1 (by pointing cursor on figure 1 and clicking). Then point cursor arrow at trace near peak and move until point 1.17 μ*s* appears; that is the end of axial phase which is also the start of the radial phase.

Note: This point occurs not at the apparent start of current dip, but a little before that. There is no distinct indication on the trace that precisely marks this point. The term rollover may be a better term suggesting a smooth merging of the axial and radial phase. The apparent current dip occurs a little after the end of the axial phase.

Next locate point 1.41 μ*s* which is the end of the radial phase. Also locate the point 1.38 μ*s* which is the start of the pinch phase. There is no clear indication on the trace to mark this point either.

Fig 2

Select Fig 2 (with cursor) and read off the pink curve that the peak axial speed reached is 6.6 *cm*/μ*s*. Confirm this on the data line; Cell P17. How many *km* per hour is this? And what is the Mach Number? 1 *cm*/μ*s*=36,000 *km*/*hr*; so 6.6 *cm*/μ*s*=237,600 *km*/*hr*

Expressing this speed in *km*/*hr* is to give an idea of how fast the speeds are in the plasma focus; it should give the idea also of temperature, since for strong shock waves (high Mach number motion) there is efficient conversion of energy from directed to thermal, i.e. from high kinetic energy to high temperature.

Mach number=speed/sound speed; finding this number is one of the questions for Exercise 1 (see below).

Fig 3
Select Fig 3. Read from dark blue curve that piston hits axis (radius=0) at 178*ns* after start of radial phase; and outgoing reflected shock (light blue) hits incoming piston (pink curve) at 210*ns* at radius of 2.1*mm*. The pinch phase starts at this 209*ns* and ends at 235 *ns* at a further compressed radius of 1.42*mm*.
Note the square of the ratio of pinching a/r_{min} is a measure of the how much the ambient density has been increased by the pinching effect.

Fig 4
Computed waveform of tube voltage during radial phase. Note the peak value of the tube voltage induced by the rapid plasma motion.

Fig 5
Select Fig 5. Note from the dark blue curve that peak radial shock speed is 20.4 *cm*/μ*s* just before the radial shock hits the axis at 178 *ns* after start of radial phase. Also read from the pink curve that peak piston speed is 14.2 *cm*/μ*s* reached just before the radial shock reaches its peak speed. Yellow curve shows column elongation speed. Note that these peak speeds are also recorded in the data line.

Other figures:
Select **Fig 6**: and read the peak temperature reached.
Select **Fig 7**: and read the various energies.
Select **Fig 8**: and read the various powers

Note that more charts are plotted on Sheet2 of **RADPFV5.15de.xls** These charts form a more complete picture of the plasma focus pinch, and may be used as starting guides for laboratory measurements of the various plasma properties.

2.5 Exercise 1: Interpreting and recording data from the worksheet.

Fill in the following blanks:

Q0: Given the speed of sound in neon at room temperature is 450 *m/s* (1600 *km/hr*), the Mach number of the peak axial phase speed, and of the peak radial phase speed (radially inwards shock speed) are _____ and _____. (Note: *The peak axial speed can be found from **Fig.2**, and the peak radial speed can be found from **Fig.5**, for this particular plasma focus operation, also recorded in the dataline*)
Q1: The peak temperature reached is _____*K*.
Q2: At that temperature the effective charge number (from small figure) is _____ and specific heat ratio has a range as follows _____.
Q3: There is a moment in time when the temperature jumps by a factor of approximately 2. This is at _____ *ns* from start of radial phase (Note: *this happens at reflected shock according to the model*)
Q4: Joule heating reached a maximum value of_____ *J*.
Q5: Total radiation reached a maximum value of_____ *J* (Note: *the – sign for the radiation energy indicates energy taken out of the plasma by emission; ignore the – sign for this measurement*)
Q6: Line Radiation reached a maximum value of _____ *J*.
Q7: Peak radiation power reaches a value of _____ *W*.

2.6 Conclusion

We had an introduction to the Worksheet of **RADPFV5.15de.xls**
We configured the UPFL as the NX2 at 11 *kV* 2.6 *Torr* neon.
We used properly fitted model parameters. (*Note: Fitting model parameters will be covered in a future session*).
We noted that the current waveform is distorted from damped sinusoid-like waveform (damped sinusoid-like waveform is the current waveform when the plasma focus is short-circuited).
We studied the computed results, including total current, tube voltage, pinch current, radial and axial trajectories, radial and axial speeds, plasma temperature and plasma Joule heating and radiation energies.
We also located various points on the current trace including: end of axial phase/start of radial phase; end of radial phase; start and end of pinch phase.

Note: This particular numerical 'shot' used properly fitted model parameters. The results of dynamics, electrodynamics and radiation as seen above are, in our experience, comparable with the actual experiments conducted at NTU/NIE.

End of Module 2.

Module 3: I. Configuring and fitting computed current to measured current
II. Comparing a large PF with a small PF-neutron yield etc
(Follow the instructions in the following notes. You may also wish to refer to the supplementary notes **SP2.doc)**

Summary

For this module we fit model parameters so that computed current waveform matches measured current waveform.

First we configure the UPFL (**RADPFV5.15de.xls**) for PF1000 operating in deuterium; using trial model parameters. We fire a shot. **We do not know how good our results are without a reference point; i.e. some comparison with experimental results.**

A total current waveform of the PF1000 has been published; we have it in digitized form in a file **PF1000data.xls**. We also have the chart of this waveform displayed in this file.
To ensure that our computed results are comparable to experimental results**,** the key step is to fit model parameters, by adjusting the model parameters until the computed total current trace matches the measured total current trace.

To do this, we add **PF1000data.xls** to our numerical focus laboratory **RADPFV5.15de.xls.** Next we plot the computed current waveform in the same chart. The model parameters are varied; at each variation the focus is fired, and the computed current waveform is compared with the measured waveform. The process is continued until the waveforms are best matched. A good match gives confidence that the computed results (trajectories, speeds, temperature, neutron and radiation yields etc) are comparable with actual experimental results.

After the guided fitting of the PF1000, we have a self exercise to fit the Chilean PF400J.
We then tabulate important results of both machines, and do a side-by-side comparison of big versus a small plasma focus to obtain important insights into scaling laws/rules of the plasma focus family.

I. Configuring and fitting computed current to measured current

3.1 Configure the code for the PF1000 using trial model parameters
3.2 Place a measured (published) PF1000 current waveform on Sheet3
3.3 Place the computed current waveform onto the same chart as the measured current waveform in Sheet3
3.4 Vary the model parameters to obtain matching of computed versus measured current traces

II. Comparing a large PF with a small PF-neutron yield etc

3.5 Exercise 2: Tabulate results for PF1000 obtained in numerical experiments
3.6 Exercise 3: Fitting the PF400J and tabulate the results for PF400J side by side with the results for PF1000, for a comparative study
3.7 Conclusion

The material

You need **RADPFV5.15de.xls** for the following work. Copy and paste a copy on your Desktop. You also need the files **PF1000data.xls**, **PF400data.xls** and **compareblank.xls** for this session. Copy and paste a copy of each file onto your desktop.

I. Configuring and fitting computed current to measured current (guided–4 hrs)

3.1 Configure the code for the PF1000 using trail model parameters

Double click on **RADPFV5.15de.xls** on your Desktop.
Security Warning "Macros have been disabled" appear at top left hand corner of Worksheet with side box "options".
Click on "options"- select the button "Enable this content"- click OK
After this procedure, the worksheet is macro-enabled and is ready for firing.

[EXCEL 2007: Security Warning "Macros have been disabled" appear at top left hand corner of Worksheet with side box "options".
Click on "options"- select the button "Enable this content"- click OK]

Type in cell B3: PF1000; for identification purposes.

The PF1000, at 40 *kV*, 1.2 *MJ* full capacity, is one of the biggest plasma focus in the world. Its 288 capacitors have a weight exceeding 30 tonne occupying a huge hall. It is the flagship machine of the ICDMP, International Centre for Dense Magnetised Plasmas.

We use the following bank, tube and operating parameters for the PF1000:

Bank:	L_0=33.5 *nH*, C_0=1332 μF, r_0=6.3 $m\Omega$
Tube:	b=16 *cm*, a=11.55 *cm*, z_0=60 *cm*
Operation:	V_0=27 *kV*, P_0=3.5 *Torr*, *MW*=4, *A*=1, *At-Mol*=2

For this exercise we do not know the model parameters. We will use the trial model parameters recommended in the code (See cells T9-V9)
Model: massf (f_m) =0.073, currf (f_c)=0.7, massfr (f_{mr}) =0.16, currfr (f_{cr}) =0.7; our first try.

Configuring: Key in the following:

	A5	B5	C5	D5	E5	F5
	33.5	1332	16	11.55	60	6.3
Then	A9	B9	C9	D9	E9	
	27	3.5	4	1	2	
Then	A7	B7	C7	D7		
	0.073	0.7	0.16	0.7	for first try	

Or follow the guide in A4-F4, to key in A5-F5 for the relevant parameters.

Fire a shot: Place the cursor in any blank non-active space, e.g. G8. (point the cursor at G8 and click the mouse). Press 'Ctrl' and 'A'. (equivalent to firing a shot)
The program runs and results are displayed in columns and also in figures.

Is our simulation any good? Not if there is no reference point!!
To assess how good our simulation is, we need to compare our computed current trace with the measured current trace, which has been published.

Note that at this point: the configured **RADPFV5.15de.xls** contains computed data for PF1000 with the trial model parameters of: massf (f_m) = 0.073, currf (f_c) = 0.7, massfr (f_{mr}) = 0.16, currfr (f_{cr}) = 0.7

3.2 Place a measured (published) PF1000 current waveform on Sheet3

3.2.1 The PF1000 current waveform is in the file **PF1000data.xls**. You now want to place this data file as an additional sheet in our **RADPFV5.15de.xls** workbook.

RADPFV5.15de.xls is already open, click on 'File' tab; drop down appears,
click on 'Open'.
Look in: Desktop; select PF1000data.xls; double click to open this file.
Click on 'Edit' tab; select 'Move or Copy Sheet'.
A window pops out; 'Move selected sheets To book'; select **RADPFV5.15de.xls**. 'Before Sheet:' select '(move to end)'. Click 'OK'.
You have copied PF1000data.xls into **RADPFV5.15de.xls** as Sheet3.

[EXCEL 2007: RADPFV5.15de.xls is open, minimize by clicking top right hand corner tab the - sign. Open **PF1000data.xls.** Locate tab Sheet3 on lower left corner of worksheet. Right click on tab Sheet3. Select move or copy to book **RADPFV5.15de.xls.** Click on (move to end). Tick Create a copy. Click OK]

3.2.2 With this procedure you have copied **PF1000data.xls** as Sheet3 in **RADPFV5.15de.xls.** The chart has already been prepared. The measured current waveform appears in the chart.

3.3 Place the computed current waveform onto the same chart as the measured current waveform in Sheet3

In the next steps we will place the computed current data from Sheet1 into this same chart in Sheet 3, by the following procedure.

Place cursor on the chart; click, then right click; drop down appears- click on source data; click on series.
In the series box click on computed current in kA; then in the box against 'X Values' type in the following string: "**=sheet1!a20:a6000**" [without the quotation marks].
Next click in the box against 'Y Values' and type in the following:
"**=sheet1!b20:b6000**" [without the quotation marks]. Click button 'OK'.

[EXCEL 2007: Position the cursor on the chart in Sheet3 containing the measured current waveform. Now **right click**. Pop-up appears. Click on Select data. Select the series "Computed current in *kA*". Click on Edit. On the new pop-up for series the name "="Computed current in *kA*" is already there.
For Series X values key in **"=Sheet1!a20:a6000"**
For Series Y values key in **"=Sheet1!b20:b6000"** Click OK; and click OK.]

The computed current waveform from Sheet1 is charted in the figure in Sheet3 with the same time scale and the same current scale.

You can now compare the computed current trace with the measured current trace.

You should see a pink trace which has just appeared on the chart. The pink trace (see figure 1 below) is the computed current trace transferred from Sheet1 (where the time data in μ*s* is in column A, from A20-A several thousand; and corresponding computed current data in *kA* is in column B, from B20 to B several thousands). We are selecting the first 5980 points (if that many points have been calculated) of the computed data; which should be adequate and suitable.

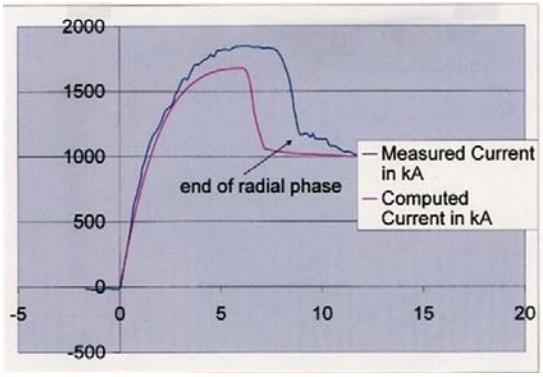

Figure 1. Comparison of traces: Note that there is very poor matching of the traces; using the first try model parameters.

3.4 Vary the model parameters to obtain matching of computed versus measured current traces

Note that bank, tube and operating parameters have all been given correctly.

3.4.1 First fit the axial phase

[*suggestion: read* **SP2.doc** *pg 3 'First step is fitting the axial phase'.*]

From the comparison chart on Sheet2,

We note: that the **computed current dip comes much too early**;
that the **computed current rise slope is only very slightly low**;
that the **computed current maximum is too low**.

All these 3 observations are consistent with a possibility that the axial speed is too fast; which would cause the radial phase to start too early. Too high an axial speed would also cause too much loading on the electrical circuit (similar to the well known motor effect) as the quantity [0.5 x dL/dt=0.5x L'x dz/dt] is a dynamic resistance loading the circuit during the axial phase; here the inductance per unit length $L'=(\mu/2\pi) \times ln(b/a)$. This too high speed would also lower the peak current.

To reduce the axial speed, we could increase the axial mass factor. We note that the axial phase ends too early by some 20%; indicating the axial speed is too fast by 20%.

In the plasma focus (as in pinches, shocks tubes and other electromagnetically driven plasma devices) speed~density$^{0.5}$. So the correction we need is to increase the axial mass factor by 40%. So try an axial mass factor of 0.073x1.4~ 0.1.

We toggle to Sheet1 by clicking on 'Sheet1' (just below the worksheet).
Click on cell A7, and type in 0.1.
Fire the focus by pressing Ctrl+A.
Program runs until completed, and results are presented.
Note TRadialStart (H11) has increased some 0.6 μs.
Toggle to Sheet3 (i.e. click on Sheet3 just below work sheet).

Note that the computed current dip is now closer to the measured current dip in time (still short by some 10%; reason being that increasing the axial mass factor reduces the speed which in turn causes a reduced loading. This increases the current which tends to increase the axial speed so that our mass compensation of 40% becomes insufficient). The value of the computed peak is also closer to the measured. So we are moving in the right direction!
But still need to move more in the same direction. Next try axial mass factor of 0.12. Toggle to Sheet1, type 0.12 in A7. Fire. Back to Sheet3. Note improvement in all 3 features.

In similar fashion, gradually increase the axial mass factor. When you reach 0.14 you will notice that the computed current rise slope, the topping profile, the peak current and the top profile are all in good agreement with the measured. The computed trace agrees with the measured trace up to the start of the dip. Note that the axial model parameters at this stage of agreement are: 0.14 and 0.7. You may wish to try to improve further by making small adjustments to these parameters. Or else go on to fit the radial model parameters.

3.4.2 Next, fit Radial phase

Note that the computed current dip is too steep, and dips to too low a value. This suggests the computed radial phase has too high a speed. Try increasing the radial mass factor (cell C7), say to 0.2. Observe the improvement (dip slope becomes less steep) as the computed current dip moves towards the measured dip.
Continue making increments to mass(f_r) (cell C7). When you have reached the mass(f_r) value of 0.4; it is becoming obvious that further increase will not improve the matching; the computed dip slope has already gone from too steep to too shallow, whilst the depth of the dip is still excessive.

How to raise the bottom of the dip? Here we suppose the following scenario:
Imagine if very little of the current flows through the pinch, then most of the total current will flow unaffected by the pinch. And even if the pinch were a very severe one, the total current (which is what we are comparing here) would show hardly a dip. So reducing the radial current fraction, ie currfr (or f_{cr}) should reduce the size of the dip.

Let us try 0.68 in cell D7. Notice a reduction in the dip. By the time we go in this direction until currfr(f_{cr}) is 0.65, it becomes obvious that the dip slope is getting too shallow; and the computed dip comes too late.

One possibility is to decrease massfr(f_{mr}) (which we note from earlier will steepen the dip slope); which however will cause the dip to go lower; and it is already too low. Another possibility is to decrease the axial phase massf(f_m), as that will also move the computed trace in the correct direction.

Try a slight decrease in axial massf (f_m), say 0.13.

Note that this change aligns the dip better but the top portion of the waveform is now slightly low, because of the increased loading on the electrical circuit by the increase in axial speed. This suggests a slight decrease to circuit residual resistance r_0 (or changes to L_0 or C_0; fitting those could be tricky, and we try to avoid unless there are strong reasons to suspect these values). Easier to try lowering r_0 first. Try changing r_0 to 6.1 $m\Omega$.

The fit is quite good now except the current dip could be steepened slightly and brought slightly earlier in time. Decrease massfr(f_{mr}), say to 0.35. The fit has improved, and is now quite good, except that the dip still goes too low. At this stage we check where we are at.

Toggle to Sheet1. Note from Sheet1 that the radial phase ends at 9.12 μs. Back to Sheet3.

Observe (using cursor) that the point 9.12 is not at the point where the computed (pink curve) dip reaches its inflection point; but some 0.02 μs before that point (see figure below). So we note that the computed curve agrees with the measured curve up to the end of the radial phase with a difference of less than 0.02 *MA* out of a dip of 0.66 *MA* (or 3%).

The fitting has already achieved good agreement in all the features (slopes and magnitudes) of the computed and measured total current traces **up to the end of the radial phase**.
Do not be influenced by agreement, or disagreement of the traces beyond this end point.

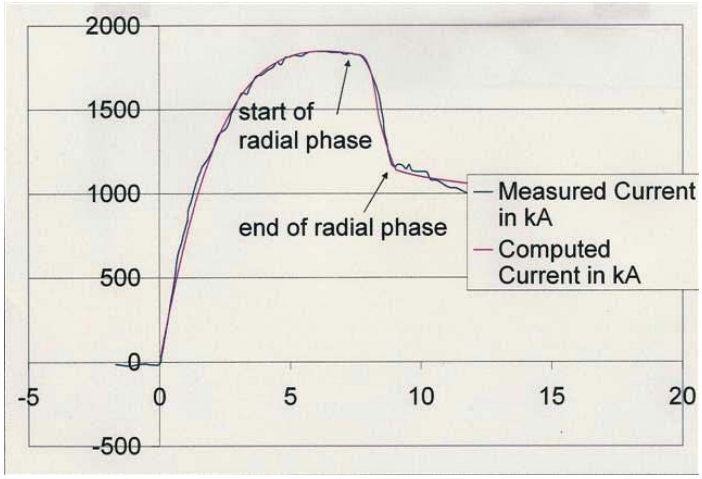

Figure 2. The best fit.

So we have confidence that the gross features of the PF1000 including axial and radial trajectories, axial and radial speeds, gross dimensions, densities and plasma temperatures, and neutron yields up to end of radial phase may be compared well with measured values.
Moreover the code has been tested for neutron and SXR yields against a whole range of machines and once the computed total current curve is fitted to the measured total current curve, we have confidence that the neutron and SXR yields are also comparable with what would be actually measured.

Having said that, those of you who have some experience with the plasma focus would note that at the end of the radial phase, some very interesting effects occur leading to a highly turbulent situation with occurrence, for example, of high density hot spots. These effects are not as yet modeled in the code. Despite this drawback, the postulated beam-target neutron yield mechanism seems able to give estimates of neutron yield which broadly agree with the whole range of machines. For example, the neutron yield computed in this shot of $1.08x10^{11}$ is in agreement with the reported PF1000 experiments.

One further note: *We have recently confirmed that the above discussion of fitting applies typically to machines with low L_0, below perhaps 60 nH. For machines above 100 nH another strategy of fitting or even modelling may need to be adopted. This is related to the comment just above this note.*

II. Comparing a large PF with a small PF - neutron yield etc

3.5 Exercise 2: Tabulate results for PF1000 obtained in numerical experiments

You have been following the guided steps in the above fitting:
Fill in the following:

Q1: My best fitted model parameters for PF1000, 27*kV*, 3.5 *Torr* deuterium are:

f_m=	f_c=	f_{mr}=	f_{cr}=

Q2: Insert an image of the discharge current comparison chart in Sheet3 here.

Q3: Fill up the following table. Use the file **compareblank.xls** for this purpose.

Parameter	PF 1000 (at 27 *kV* 3.5 *Torr* D_2)
Stored Energy E_0 in *kJ*	
Pressure in *Torr*, P_0	
Anode radius a in *cm*	
$c=b/a$	
anode length z_0 in *cm*	
final pinch radius r_{min} in *cm*	
pinch length z_{max} in *cm*	
pinch duration in *ns*	
r_{min}/a (r_{min} is also called a_{min})	
z_{max}/a	
I_{peak} in *kA*	
I_{peak}/a in *kA/cm*	
$S=(I_{peak}/a)/(P_0^{1/2})$(*kA/cm*)/*Torr*$^{1/2}$	
I_{pinch} in *kA*	
I_{pinch}/I_{peak}	
Peak induced voltage in *kV*	
peak axial speed in *cm*/μ*s*	
peak radial shock speed *cm*/μ*s*	
peak radial piston speed *cm*/μ*s*	
peak temperature in 10^6 *K*	
neutron yield in units of 10^6	

[*After filling, save this Excel sheet you will use the same Excel sheet to fill in the results for PF400J which is the subject of the next exercise.*]

3.6 Exercise 3: Fitting the PF400J and tabulate results for PF400J side by side with the results for PF1000 for a comparative study

Participants are to fit computed current to measured current waveform of PF400J (bank, tube and operating parameters all correctly given)

In Module 2, we worked with the Singaporean NX2; a 3kJ neon plasma focus designed for SXR lithography. For our first fitting exercise we worked with the Polish PF1000, one of the largest plasma focus (MJ) in the world. You are now given data for the PF400J, a small sub-kJ plasma focus operated in Chile at the Atomic Energy Commission, for the specific purpose of investigating small focus devices. [Note: The 1000 in PF1000 refers to kJ. The 400 in PF400J refers to J; so the energy ratio of the PF1000 to the PF400J is: 1,200,000/400~3000]. The PF400J is a small table top device with all components fitting on a small table top. The PF1000 has a huge chamber and its capacitor bank fills a whole big hall.

Given: the current waveform data of the PF400J, digitized from a published waveform. The data is in the file **PF400data.xls.**

Your task: is to fit model parameters until the computed current waveform matches the measured waveform. Some guidance is given below.

Suggested steps to fit PF400J

i. **Make a clean copy** of **RADPF05.15de.xls** from your Reserve folder to your Desktop. Open this file.

ii. **Copy PF400data.xls** as Sheet3 of **RADPF05.15de.xls using procedure as in section 3.2.1 above**. **The measured waveform is already pre-charted.**

iii. **Transfer computed current data from Sheet1 onto the measured current chart in Sheet3**; as in step in section **3.3** above using strings: "**=sheet1!a20:a6000**" [without the quotation marks] and "**=sheet1!b20:b6000**" [without the quotation marks]. No trace of computed current appears yet, since we have not yet 'fired' PF400J.

Write down the bank, tube and operating parameters (from the table in the lower part of Sheet3, NOT from the top line, which contains some nominal values). Toggle to Sheet1.

iv. **Configure the Universal Plasma Focus with the following bank, tube and operating parameters**

$L_0(nH)$	$C_0(\mu F)$	$b(cm)$	$a(cm)$	$z_0(cm)$	$r_0(m\Omega)$
40	0.95	1.55	0.6	1.7	10
massf	currf	massfr	currfr	model parameters	
$V_0(kV)$	$P_0(Torr)$	*MW*	*At No.*	*At1;Mol2*	Operation Parameters
28	6.6	4	1	2	

Key in the first try model parameters; *[scroll a little to the right and use the suggested parameters for the UNU ICTP PFF, cells T9-V9]*.

v. **Fire PF400J**; and see the comparative results by toggling to Sheet3.

vi. **Fitting the computed current waveform to the measured waveform**

vii. **Suggested first steps:** Fit the axial region by small adjustments to f_m and f_c, where necessary. In fitting the axial phase, the more important region to work on is the **later part of the rising slope and the topping profile towards the end of the axial phase**. So each time you should note the position of the end of the axial phase from Sheet1 and locate that position on the chart in Sheet2, using the cursor.

viii. **Final steps:** When you have done the best for the axial phase up to the end of the axial phase, then proceed to fit the radial phase. Tip: The dip for the PF400J is not very dramatic. **Enlarge** the trace so the rollover and the dip can be more clearly compared.

Fill in the following questions, copy and paste and e-mail to me.

Questions

Q1: My best fitted model parameters for PF400J, 28 *kV*, 6.6 *Torr* deuterium are:

f_m=	f_c=	f_{mr}=	f_{cr}=

Q2: Insert an image of the discharge current comparison chart in Sheet3 here.

Q3: Complete the Excel Sheet which you started in the last Exercise; to compare a BIG (~500 *kJ*) plasma focus with a small one (~400*J*). As you fill up, note particularly each group of ratios (each group is denoted by a different colour). Note particularly the order of magnitude of the ratios. *[use the Excel sheet, rather than this table]*.
The ratios below were calculated from the actual PF1000 and PF400J results; and left here as a check for you. Calculate your own ratios from your own results. At the end of the exercise save this Excel Sheet as **PFcomparison.xls**. It will be used again if eventually you go to the more advanced exercises of Modules 5.

Make up the following table comparing a BIG plasma focus with a small plasma focus

Parameter	PF1000 (at 27*kV* 3.5 *Torr* D_2)	Ratio PF1000/PF400J	PF400J (at 28*kV* 6.6 *Torr* D_2)
Stored Energy E_0 in *kJ*	486	1313	0.37
Pressure in *Torr*, P_0	3.5	**0.53**	6.6
Anode radius a in *cm*	11.55	**19.3**	0.6
$c=b/a$	1.39	**0.54**	2.6
anode length z_o in *cm*	60	**35.2**	1.7
final pinch radius r_{min} in *cm*		**26.7**	
pinch length z_{max} in *cm*		**22.2**	
pinch duration in *ns*		**53**	
r_{min}/a		**1.4**	
z_{max}/a		**1.16**	
I_{peak} in *kA*		**14.6**	
I_{peak}/a in *kA/cm*		**0.76**	
$S=(I_{peak}/a)/(P_0^{1/2})$(*kA/cm*)/*Torr*$^{1/2}$		**1.05**	
I_{pinch} in *kA*		**9.64**	
I_{pinch}/I_{peak}		**0.65**	
Peak induced voltage in *kV*		**2.4**	
peak axial speed in *cm*/μs		**1.24**	
peak radial shock speed *cm*/μs		**0.48**	
peak radial piston speed *cm*/μs		**0.48**	
peak temperature in $10^6 K$		**0.19***	
neutron yield Y_n in 10^6		81920	
Measured Y_n in 10^6: range	(2 - 7)E+03		0.9-1.2
Measured Y_n in 10^6 :highest	2.0E+04		

We could then use the tabulation for several applications including the following: Think of scaling rules, laws:

Q4: What is the significance of the Speed Factors *S* of PF1000 and PF400J? Which one's temperature should be higher?

***The ratio radial speed/axial speed is:

$$v_r / v_a = \left[\frac{(c^2 - 1)(\gamma + 1)}{4 \ln c} \right]^{1/2}$$

Note: http://www.plasmafocus.net/; download the Theory of the model

3.7 Conclusion

In this module we have learned how to fit a computed current trace with a measured current waveform, given all bank, tube and operational parameters. For the PF1000 we obtained a good fit of all features from the start of the axial phase up to the end of the radial phases; giving confidence that all the computed results including trajectories and speeds, densities, temperatures and neutron and radiation yields are a fair simulation of the actual PF1000 experiment.

We also fitted the computed current to the measured current of the PF400J; thus computing its dynamics and plasma characteristics and neutron yield.

We tabulated important results of the two machines side by side.

We noted important physics:

Although the machines differ greatly in storage energy and hence in physical sizes, the **speed factor *S* is practically the same**. This has given rise to the now well-known observation that all plasma focus, big and small, all operate with essentially the same energy per unit mass when optimized for neutron yield. See e.g.: http://en.wikipedia.org/wiki/Dense_plasma_focus

The axial speed is also almost the same; in which case the radial speeds would have been almost the same, except they (the radial speeds) are influenced by a geometrical factor $\mathbf{[(c^2-1)/\ln c]^{0.5}}$. For these 2 machines the factors differ by 1.5; hence explaining the **higher radial speeds in PF400J**; and also the **higher temperatures** in the smaller PF400J.

The **pinch dimensions scale with *'a'*** the anode radius. The **pinch duration also scales with *'a'*, modified by the higher *T*** of the PF400J, which causes a higher small disturbance speed hence a smaller small disturbance transit time. In this model this transit time is used to limit the pinch duration.

Finally we may note that just by numerical experiments we are able to obtain extensive properties of two interesting plasma focus machines apparently so different from each other, one a huge machine filling a huge hall, the other a desk top device. Tabulation of the results reveals an all important characteristic of the plasma focus family. They have essentially the same energy per unit mass (*S*).

A final question arising from this constant energy/unit mass: Is this at once a **strength** as well as a **weakness** of the plasma focus?

End of Module 3.

Module 4: PF1000 neutron yield versus pressure
(Follow the instructions in the following notes. You may also wish to refer to the supplementary notes **SP3.doc**)

Summary

This module looks at variation of neutron yield with pressure; running PF1000 from short-circuit (very high pressure), through optimum pressure to low pressure. The very high pressure of the short-circuit shot stops all current sheath motion thus simulating a short circuit. The aim of this shot is just to obtain short-circuit current waveform for comparison with the focusing waveforms at different lower pressures. When the operating (ambient) pressure is low enough neutrons are emitted. The variation of the yield and other properties with pressure are compiled together, and presented on one chart in normalized form. In this way correlation of various quantities may be seen.

4.1 Configure the code for the PF1000 at 27 *kV*, 3.5 *Torr* D_2 using model parameters which we had fitted earlier
4.2 Fire the PF1000 at very high pressure, effectively a short circuit
4.3 Fire the PF1000 at lower pressures from 19 *Torr* down to 1 *Torr*; looking for optimum neutron yield
4.4 Exercise 4: Place the current waveforms (from section 4.3) at different pressures on the same chart for comparative study
4.5 Exercise 5: Tabulate results at different pressures for comparative study; including speeds, pinch dimensions, duration, temperature and neutron yield
4.6 General notes on fitting, yield scaling and applications of the Lee model code

The material
You need **RADPFV5.15de.xls** for the following work. Copy and Paste on your Desktop. You also need the files **PF1000pressureblank.xls.** This file contains also tabulation blanks for your convenience.

4.1 Configure the code for PF1000 at 27 *kV*, 3.5 *Torr* deuterium using model parameters which we had fitted earlier

i. Preparing Sheet3

Open **RADPFV5.15de.xls;** copy **PF1000pressureblank.xls** as Sheet3; using procedure which we have practiced in Module 3.
Examine Sheet3

PF1000pressureblank.xls, copied as Sheet3 has the parameters of PF1000 recorded along the top rows. One set of measured time-current data is supplied at Columns A and B. To save participants some time, time-current data for several traces are already computed and filled in: 3.5 *Torr* at columns C and D; 19 *Torr* at columns G & H; 7.5 *Torr* at columns M & N and 1 *Torr* at columns S & T. These are already plotted in figure 1. You are required to fire shots at several other pressures and copy the time-current data for these shots onto the columns reserved for these shots. In this way you fill up the charts with sufficient traces to cover the optimum pressures for neutron yield. These pressures are 100,000, 14, 10, 6 and 2 *Torr*.
Scrolling to the right you see table 1 with plasma focus properties at various pressures. The properties corresponding to the shots at 19, 7.5, 3.5 and 1 *Torr* are already filled in. Data from those other shots to be fired by the participants are to be filled in to complete the table. Below table 1 is table 2 with data normalized from table 1 using the shot at 7.5 *Torr as* the reference shot for normalizing.
Figure 2 displays the normalized Y_n, I_{peak}, I_{pinch} and radial phase piston work EINP *versus* pressures from table 2.
[*Note that the curves in figure 2 have places where they all come to zero. That is because the table has not been filled for those shots yet to be fired. For these shots the data points have been put to zero. The curves will take on their correct shapes once the data has been correctly filled in. This is the job for the participant*]

ii. Configure the code for PF1000

Use the data in PF1000 pressureblank.xls to configure.

Bank:	L_0=33.5 *nH*, C_0=1332 μF, r_0=6.1 $m\Omega$
Tube:	b=16 *cm*, a=11.55 *cm*, z_0=60 *cm*
Operation:	V_0=27 *kV*, P_0= ? *Torr*, *MW*=4, *A*=1, *At-Mol*=2
Model:	f_m=0.13, f_c=0.7, f_{mr}=0.35, f_{cr}=0.65

4.2 Fire the PF1000 at very high pressure, effectively a short circuit

Key in 100,000 *Torr* at B9.
[*Note: In the laboratory it is of course impossible to fire such a shot and a physical short-circuit may need to be used at the insulator end of the plasma focus; or fire at the highest safe pressure in argon. In the lab we have used 50 Torr argon, to obtain very approximate results.*]
[*In the numerical experiment at this high pressure the current sheath only moves a little down the tube, adding hardly any inductance or dynamic loading to the circuit. So it is equivalent to short-circuiting the plasma focus at its input end. In the code there is a loop during the axial phase, computing step- by- step the variables as time is incremented. The*

loop is broken only when the end of the anode (non-dimensionalised z=1) is reached. In this case we do not reach the end of the anode. However there is an alternative stop placed in the loop that stops the run when time reaches nearly 1 full cycle is completed (non-dimensionalised time=6 ie nearly 1 full cycle time, 2π, of the short- circuited discharge).
At the start of the run, the code computes a quantity ALT= ratio of characteristic capacitor time to sum of characteristic axial & radial times. Numerical tests have shown that when this quantity is less than 0.65, the total transit time is so large (compared to the available current drive time) that the radial phase may not be efficiently completed. Moreover because of the large deviation from normal focus behaviour, the numerical scheme and 'house keeping' details incorporated into the code may become subjected to numerical instabilities leading to error messages. To avoid these problems a time-match guard feature has been incorporated to stop the code from being run when ALT<0.65. When this happens one can over-ride the stop; and continue running unless the run is then terminated by Excel for e.g. 'over-flow' problems. In that case one has to abandon the run and reset the code.]

Fire the high pressure shot. The pressure is too high for a normal run and we are automatically toggled over to the Macro; the Visual Basics Code appears at Statement 430 Stop; with a warning message that pressure is too high. In this case we know what we are doing, and over-ride as follows: Click on 'Run' (above the code sheet), and 'continue'. Another 'Stop' appears just below line 485; with a warning about transit time. Click on 'Run' and 'continue'; another 'Stop' appears below Line 488. Click on 'Run' and 'Continue'.

In a little while the run has proceeded and finally the statement "If T > 6 Then Stop" appears; indicating we have completed nearly one cycle of the capacitor discharge; and reached the pre-set time limit.

Now, locate the 'x' at the extreme right hand corner of the screen. Click on this 'x'; pop-up appears with the message 'This command will stop the debugger'. Click on OK, which toggles us back to the worksheet, Sheet1.

Copy the data in columns A & B from A20 and B20 to the end of the computed current data (several thousand cells down); toggle to Sheet3 and 'paste' the copied time-current data onto Columns E & F (in the labeled space provided in Sheet3. Locate table 1 by scrolling to the right. Fill in the value of I_{peak} [read from figure 1 or from the relevant cell of the dataline] onto the table 1 against 100,000 *Torr*. Put zero against all the other quantities (I_{pinch}, peak v_a, S, peak v_s …. T and Y_n….)

4.3 Fire the PF1000 at lower pressures from 19 *Torr* down to 1 *Torr*, looking for optimum neutron yield

Fire the next shot at 14 *Torr*. As the ALT value is over 0.65, the run proceeds as normal. Copy the time-current data from Columns A & B (from rows 20 down) to Sheet3 columns I & J. Fill in the table 1 [$I_{peak,}$ I_{pinch}, peak v_a, S, peak v_s … T… Y_n…n_i & EINP taken from the data line) for the data from shot 14 *Torr*.

Repeat for pressures **10**, 9, 8, 7.5 , 7, **6**, 3.5 , **2** and 1 *Torr*; tabulating the data for all these shots onto table 1; but copy and paste the time-current data for only selected shots of 14, 10, 6 and 2 [in order for figure 1 not to become too crowded]. The list of pressures had been

chosen as above in order to demonstrate the way the neutron yield varies with pressure. It is clear that Y_n increases rapidly from 14 *Torr* to 10 *Torr*. More points are chosen between 10 *Torr* and 6 *Torr* and it is obvious that the optimum pressure (for Y_n) is between 8 *Torr* and 7 *Torr*. The participant will notice this as the shots are fired and as the Y_n data is copied on to the table 1.

4.4 Exercise 4: Place the current waveforms (from section 4.3) at different pressures on the same chart for comparative study

Suggested procedure: To save you time, the comparison chart, figure 1 has already been created for you, and pre-filled with several waveforms namely 19, 7.5, 3.5 and 1 *Torr*. You only have to fill in the ones for 100,000 and 14, 10, 6 and 2 *Torr* in the correct columns indicated by the column headings already placed on Sheet3.

You will note that the computed current waveform for 3.5 *Torr* falls neatly on the measured current waveform (as you have seen during an earlier exercise precisely with this PF1000 27 *kV*, 3.5 *Torr* current waveform.) You will recognize that we are using the computed 3.5 *Torr* shot to fit our UPFL to the PF1000 to obtain the model parameters for the PF1000.
Thereafter the assumption is that the model parameters apply for all the other shots.
It would of course be better if for every pressure or every shot we have a measured current trace to fit the code. However despite this assumption about the model parameters, the numerical experiment does show some very interesting features as we proceed below.

4.5 Exercise 5: Tabulate results at different pressures for comparative study; including speeds, pinch dimensions, duration, temperature and neutron yield

This tabulation has already been done as step (4.3) proceeded above.

In order to chart some of the computed data on one comparative chart, as mentioned already, as you fill in table 1, table 2 is at the same time filled in with each data column normalized to the data at 7.5 *Torr*, which was found to be the pressure with the highest Y_n. Thus the values of all the data in the normalized table is in the region of 1.
Plot normalized Y_n, I_{peak}, I_{pinch}, and radial EINP against P_0.

[*As you fill in table 1, the normalized quantities are automatically computed, and the chart begins to take the correct shape. At the start the chart is in a jumble because many points have not been filled in, and thus there are erratic zero points all over the place.*]

Discussion

Note 1
Look at the change of current waveforms from very high pressures to low pressures. At very high pressures the waveform is a damped sinusoid. At 19 Torr the characteristic flattening of the current waveform due to dynamics is already clearly evident. The current peak comes earlier and is lower than the unloaded (high pressure) case, the current then droops until the rollover into the dip (due to the increased radial phase loading) at around 15 μs. At lower pressures these characteristics remain the same except that the current trace is depressed more and more as speed increases. The peaking (reaching maximum current) also comes earlier and earlier, as does the radial phase rollover of the current trace. This is

characteristic of an L-C-R circuit with increasing resistance R, as R increases from light towards critical damping.

At 2.6 Torr, there is hardly any droop, the current waveform showing a distinct flat top leading to the rollover. At 1 Torr the axial speed is now so high that the axial phase is completed in less than 5 μs and the current is still rising when it is forced down by the radial phase dynamics.

Note 2

A very important point to note in neutron scaling is that there exists some confusion and even misleading information in published literature because of sloppy practice with regards to I_{peak} and I_{pinch}. These quantities are sometimes treated as one and the same or when a distinction is attempted there is then confusion between the total current at the time of pinch and I_{pinch}. For example in the case of PF1000, there appears to be some disappointment (in their publications) that (at 35 kV) with the current at more than 2 MA, Y_n is still at best in the mid 10^11; and not at least an order of magnitude higher that one might expect for currents around 2 MA. However if you numerically run PF1000 at 35 kV you will find that I_{pinch} is only 1 MA; so we are not surprised that the measured yield is at best an order of magnitude down from what you would expect thinking that your current is around 2 MA. (scaling at $Y_n \sim I^4$, a factor of 2 in current gives a factor of 16 in the yield; at $Y_n \sim I^3$, a factor of 8). So it is important that the thinking of yield should be in terms of I_{pinch} as the relevant scaling parameter. When using this model code, the distinction of I_{pinch} and I_{peak} is clear.

Next we look at the detailed tabulations: As P_0 decreases, I_{peak} decreases, and continues to decrease, because the increasing axial speed increases the circuit loading, throughout the whole range of pressures. However it is noticed that I_{pinch} increases from high pressures, peaking in a flat manner at 6 *Torr* and then decreases sharply as pressure is reduced towards 1 *Torr*. One factor contributing to the increase is the shift of the pinch time from very late in the discharge (when discharge current has dropped greatly) to earlier in the discharge (when current has dropped less). That is the main factor for I_{pinch} increasing despite a decreasing I_{peak}. At low pressures (e.g. 1 *Torr*), the radial phase now occurs so early that it is forcing the current down early in the discharge. That lowers both the I_{peak} as well as the I_{pinch}. These points are clear when you look at the comparative chart of current traces at various pressures.

The radial EINP follows the same pattern as I_{pinch}, and for the same reasons. The radial EINP computes the cumulative work done by the current sheath (piston) in the radial phases.

Looking at the other quantities, we note that the speeds (axial, radial shock and radial piston) and temperature all continue to rise as pressure lowers; similarly S and maximum induced voltage V also increase as pressure is decreased. Pinch length z_{max} is almost a constant. Minimum pinch radius and pinch duration continue to decrease; the former due to better compression at higher speeds and the latter due to the increased T. The number density progressively drops, due to the decreasing starting numbers, despite the increasing compression.

From the tabulations of the above numerical experiments, it might be useful to consider the beam-target mechanism which we are using to compute the neutron yield. This is summarized in the following note.

Note 3
(Taken from SP3.doc)
$Y_{b\text{-}t} = C_n\, n_i\, I_{pinch}^{\ 2} z_p^{\ 2} (\ln(b/r_p)) \sigma / V_{max}^{\ 1/2}$
where σ is the D-D fusion cross section. In the range we are considering we may take $\sigma \sim V_{max}^{\ n}$ where n~2-3; say we take n=2.5; then we have

$$Y_{b\text{-}t} \sim n_i\, I_{pinch}^{\ 2} z_p^{\ 2} (\ln(b/r_p))\, V_{max}^{\ 2}$$

The factor $z_p^{\ 2}(\ln(b/r_p))$ is practically constant.
Thus we note that it is the behaviour of n_i , I_{pinch} and V_{max} as pressure changes that determines the way Y_n increases to a maximum and then drops as pressure is changed.

An additional experiment is suggested, in which you can see how numerical experiments on Y_n *versus* operating pressure compare with measured results in the case of PF400J. This is discussed in Module 7.

4.6 General notes on fitting, yield scaling and applications of the Lee model code

On fitting: In the numerical experiments we soon learn that one is not able to get a perfect fit; in the sense that you can defend it as absolutely the perfect fit. The way to treat it is that one has got a working fit; something to work with; which gives comparable results with experiments; rather than perfect agreement. There is no such thing anyway; experiments in Plasma Focus (i.e. on one PF under consistent conditions) give a range of results; especially in yields (factor of 2-5 range is common). So a working fit should still give results within the range of results of the hardware experiment.

Even though a fit may only be a 'working' fit (as opposed to the hypothetical perfect fit) when one runs a series of well planned numerical experiments one can then see a trend e.g. how properties, including yields, change with pressure or how yields scale with I_{pinch}, or with L_0 etc. And if carefully carried out, the numerical experiments can provide, much more easily, results just like hardware experiments; with the advantage that after proper reference to existing experiments, then very quickly one can extend to future experiments and predict probable results.

On scaling: Data used for scaling should be taken from yield-optimized (or at least from near optimized) situations. If one takes from the worst case situations e.g. way out in the high pressure or low pressure regions, the yield would be zero for a non-zero I_{pinch}. Such data would completely distort the scaling picture.
Not only should the pressure be changed, but there should be consideration for e.g. suitable (or even optimized) I_{pinch}/a; as the value of I_{pinch}/a would affect the pressure at which optimized S is achieved.

On directions of work and applications: Efforts on the model code may be applied in at least two directions. The first direction is in the further development of the code; e.g. trying to improve the way the code models the reflected shock region or the pinch region.

The second direction is to apply the model to provide a solution to a particular problem. An example was when it was applied to look at expected improvements to the neutron yield of the PF1000 when L_0 is reduced.

Using the model code it was a relatively easy procedure, firing shots as L_0 was reduced in steps; optimizing the various parameters and then looking for the optimized neutron yield at the new value of L_0. When this exercise was carried out in late 2007, for PF1000 at 35 *kV*, unexpectedly it was found that as L_0 was reduced from 100 *nH* in steps, in the region around 35 *nH*, I_{pinch} achieved a limiting value; in the sense that as L_0 was reduced further towards 5 *nH*, whilst I_{peak} continued to increase to above 4 *MA*, I_{pinch} dropped slightly from its maximum value of 1.05 *MA* to just below 1 *MA*. This Pinch Current Limitation Effect could have considerable impact on the future development of the plasma focus.

On numerical experiments to enhance experience and intuition: Moreover the relationship between I_{peak} and I_{pinch} is implicit in the coupling of the equations of circuit and motion within the code which is then able to handle all the subtle interplay of static and dynamic inductances and dynamic resistances and the rapid changes in distributions of various forms of energies within the system. Whilst the intuitive feel of the experienced focus exponents are stretched to the limit trying to figure out isolated or integrated features of these interplays, the simplicity of the underlying physics is captured by the code which then produces in each shot what the results should be; and over a series of shots then reveal the correct trends; provided of course the series is well planned.
So the code may also be useful to provide the numerical experimenter time-compressed experience in plasma focus behaviour; enhanced experience at much reduced time. At the same time the numerical experimenter can in a day fire a number of different machines, without restrictions by time, geography or expense. The problem then becomes one of too much data; sometimes overwhelming the experience and intuition of the numerical experimenter.

On versatility: Your numerical experiments have included examining plasma focus behaviour comparing BIG, medium size and small plasma focus, looking for common and scalable parameters. You studied neutron yields as functions of pressure, comparing computed with experimental data. In 4 modules involving some 12 hours of hands-on work you have ranged over a good sampling of plasma focus machines and plasma focus behaviour.

This was all done with one code the **RADPFV5.15de.xls** the universal plasma focus laboratory facility. We should have the confidence that if we explore the open experiments suggested in the last module of the advanced course below, that could lead us to new areas and new ideas.

End of Module 4- End of Basic Course in Plasma Focus Numerical Experiments
[Comments and interaction on the course work and other matters related to plasma focus are welcome at anytime]

Reference to this course and the Lee model code should be given as follows:

Lee S. Radiative Dense Plasma Focus Computation Package (2011): RADPF www.plasmafocus.net http://www.intimal.edu.my/school/fas/UFLF/

Also see list of papers at the end of Module 1 above.

Sor Heoh Saw and Sing Lee in collaboration with Erol Kurt

IPFS

knowledge should be freely accessible to all

Institute for Plasma Focus Studies

Internet Workshop on Numerical Plasma Focus Experiments

Description of Radiative Dense Plasma Focus Computation Package RADPFV5.13.9 - S Lee Model

(Supplementary Notes for Modules 2 & 3)

Features

- **Numerical Experimental Facility**
- **Simulates any Mathers-type plasma focus, computes dynamics**
- **Design new plasma focus machines**
- **Thermodynamics included; 4 gases: H_2, D_2, Ne, Ar, Xe and He**
- **Model parameters to fit experimental axial, radial phase times**
- **Radiative phase computes line radiation, recombination and total yield. Computes neutron yield for deuterium operation; based on an improved beam-target model, calibrated at an experimental point. Plasma Self-absorption based on revised equations presented in File 3; appendix by N A D Khattak.**

Also includes:

Time guard feature

Choice of Tapered electrode

Quick choice of specified machines; one click loading of chosen machine; at present 3 machines may be click-loaded: the UNU/ICTP PFF, the NX2 and the PF1000

There are altogether 4 files in this package.
File1: PDF File "Description of Radiative Dense Plasma Focus Computation Package"
File2: PDF File "Theory of Radiative Plasma Focus Model"
File3: PDF file "Appendix by N A D Khattak".
File7: EXCEL file containing the ACTIVE SHEET AND THE PROGRAMME CODE. "Radiative Dense Plasma Focus Computation Code" RADPFV5.14

In addition, there are files for the computation of thermodynamic data needed for this code.

Hint for downloading the EXCEL FILE: Instead of left click to open the file; it is better to right click and select "save target as"; then choose a suitable location e.g. desktop. The saved EXCEL file will be only about 1M. (see last page for more hints on saving/copying)

These files may be downloaded from the following URL:

http://www.intimal.edu.my/school/fas/UFLF/

Introductory description

A simple 2 phase (axial and radial) model was developed by S.Lee in 1983 as a component of a 3kJ plasma focus experimental package which became known as the UNU/ICTP PFF. This network of basically identical 3kJ PF machines, with different experimental and application emphases, is now operated by groups in countries including Singapore, Malaysia, Thailand, India, Pakistan,, Egypt and Zimbabwe.

The model was written as a 3 phase (non-radiative) model (in GWBASIC) for an experimental program at the 1991 Spring College in Plasma Physics at the ICTP.

The present 5-phase package (axial, radial inward shock, radial reflected shock, slow compression radiative and expanded large column phase) is re-written in Microsoft EXCEL VISUAL BASIC in order to make it available for wider usage.

The model may be adapted to any conventional Mather-type plasma focus by input of machine parameters: inductance, capacitance, electrode radii and length. And operating parameters: charging voltage and fill gas pressure. The thermodynamics (specific heat ratio and charge number as functions of temperature) are included for 6 gases namely hydrogen, deuterium, neon, argon and helium and xenon. The gases may be selected by simply inputting atomic number, molecular weight and dissociation number (2 for deuterium and hydrogen, 1 for the others).

The model has been used in many PhD and Masters Theses. It has also been used for various applications, for example, in the design of a cascading plasma focus (1991); and for estimating soft x-ray yield for the purpose of developing a SXR

source for microelectronics lithography (1997). More recently the code has been used to compute pinch current from measured total current waveform (2008). With this technique numerical experiments were run to obtain neutron scaling laws (2008). Use of the code also uncovered a Plasma Focus Pinch Current Limitation Effect (2008).

Five phases of the plasma focus are simulated by the Model code:

1 Axial Phase

2 Radial Inward Shock Phase

3 Radial Reflected Shock Phase

4 Slow Compression (Radiative) Phase

5 Expanded Column Axial Phase

The phases are illustrated by Fig 1 and Fig 2. More details may be obtained from:

http://www.intimal.edu.my/school/fas/UFLF/

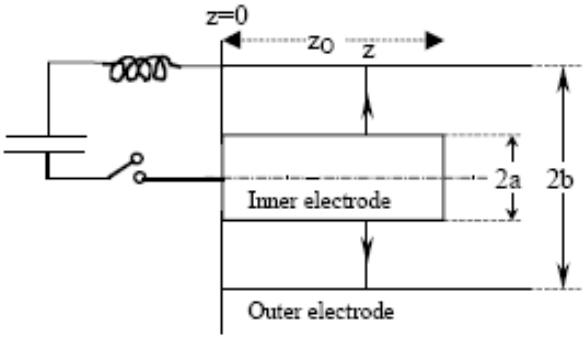

Fig 1 (a) Axial Phase

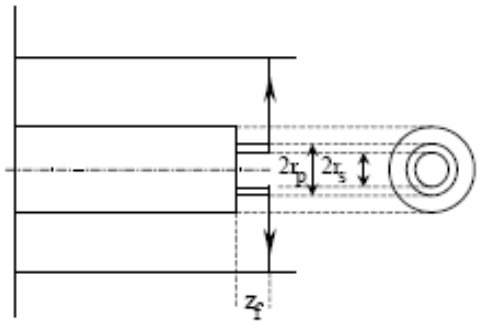

Fig 1 (b) Radial Phase

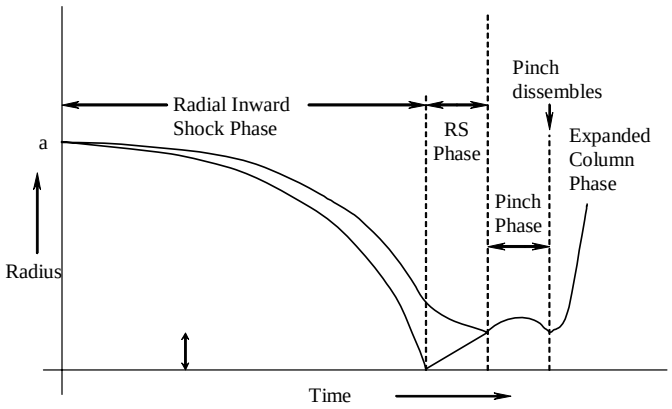

Fig 2. Schematic of radial phases

The five phases are summarised as follows (Theory and equations may be obtained from file 2 above):

1. Axial Phase: Described by a snowplow model with an equation of motion (incorporating axial phase model parameters: mass and current factors f_m and f_c) which is **coupled** to a circuit equation
2. Radial Inward Shock Phase (See Fig 1): Described by 4 **coupled** equations using an elongating slug model. The first equation computes the radial inward shock speed from the driving magnetic pressure. The second equation computes the axial elongation speed of the column. The third equation computes the speed of the current sheath, also called the magnetic piston, allowing the current sheath to separate from the shock front by applying an adiabatic approximation. The fourth is the circuit equation. The model parameters, radial phase mass and current factors f_{mr} and f_{cr} are incorporated in the radial phases. Thermodynamic effects due to ionization and excitation are incorporated into these equations, these effects being important for gases other than hydrogen and deuterium. Temperature and number densities are computed during this phase. A communication delay between shock

front and current sheath due to the finite small disturbance speed is crucially implemented in this phase.

3. Radial Reflected Shock (RS) Phase: When the shock front hits the axis, because the focus plasma is collisional, a reflected shock develops which moves radially outwards, whilst the radial current sheath piston continues to move inwards. Four coupled equations are also used to describe this phase, these being for the reflected shock moving radially outwards, the piston moving radially inwards, the elongation of the annular column and the circuit. The same model parameters f_{mr} and f_{cr} are used as in the previous radial phase. The plasma temperature behind the reflected shock undergoes a jump by a factor nearly 2.
4. Slow Compression (Quiescent) or Pinch Phase: When the out-going reflected shock hits the in-going piston the compression enters a radiative phase in which for gases such as neon,. radiation emission may actually enhance the compression where we have included energy loss/gain terms from Joule heating and radiation losses into the piston equation of motion. Three **coupled** equations describe this phase; these being the piston radial motion equation, the pinch column elongation equation and the circuit equation, incorporating the same model parameters as in the previous two phases. Thermodynamic effects are incorporated into this phase. The duration of this slow compression phase is set as the time of transit of small disturbances across the the pinched plasma column. The computation of this phase is terminated at the end of this duration.
5. Expanded Column Phase: To simulate the current trace beyond this point we allow the column to suddenly attain the radius of the anode, and use the expanded column

inductance for further integration. In this final phase the snow plow model is used, and two coupled equations are used similar to the axial phase above. This phase is not considered important as it occurs after the focus pinch.

[Note: Transition from Phase 4 to Phase 5 is observed to occur in an extremely short time. This is an important transition which merits efforts to include into the model. It would be an important next step]

Using the Code

Configuring the code

The code may be configured to any Mather-type plasma focus by inputting machine (bank and tube) parameters: inductance, capacitance, electrode radii and length; and operating parameters: charging voltage and fill gas pressure. The thermodynamics (specific heat ratio and charge number as functions of temperature) are included for 6 gases namely hydrogen, deuterium, neon, argon and helium and xenon. The gases may be selected by simply inputting atomic number, molecular weight and dissociation number (2 for deuterium and hydrogen, 1 for the others.

With the bank, tube and operating parameters specified; what remains is to specify the model parameters. As a first trial we may use: f_m=0.08, f_c=0.7, f_{mr}=0.15, f_{cr}=0.7.

Then we may run the code. The results are the following: waveforms for the total discharge current and tube voltage, axial phase trajectory and speed, radial trajectories for the shock front, current sheath and column length and the corresponding speeds, plasma temperature and radiation yields (Bremsstrahlung, line and recombination) and power; and thermodynamic quantities such as specific heat ratios and charge numbers. These are output in graphical as well as tabular forms. Also computed are plasma pinch current and neutron yield, and energy distributions, if required.

Note: **on the chronology of the development of the Lee model code**

1983: 2-phase model developed and presented by S Lee at the Spring College on Radiations in Plasmas, ICTP Trieste published in "Radiations in Plasmas" B McNamara, World Scientific pp 978-87; used in the development of the UNU/ICTP PFF and UNU, ICTP training programs and Colleges (1984, 1986 to 1991); used in PhD theses (T.Y.Tou 1986, K.H.Kwek 1988, J Ali 1990, S Mulyodrono 1993, A Serban 1995)

1991: Extension to 3-phase model (S Lee IEEE Trans Plasma Sci 1991); used for experimental program at the 1991 Spring College in Plasma Physics at the ICTP

1995: Implementation of finite small-disturbance speed correction in the radial shock phase first used in PhD thesis (Liu 1997). This is a major feature in the Lee model code.

Before this physics was implemented, radial speeds were a factor of nearly 2 too high compared with experiments. Completion of 5-phase model; used in other PhD theses (G Zhang 1999, B Shan 2000).

2000 After discussions with P Lee with a view to wider usage, the code was completely re-written in 2000 in Excel Visual Basics. Used in several recent PhD's since, notably (A Patran, D Wong, T Zhang) and in many papers. From 2003 onwards, plasma self-absorption and anode taper incorporated. Extension to Xenon.

2007 onwards: Intensive discussions with S H Saw (INTI UC) , P Lee (NTU/NIE), R S Rawat (NTU/NIE) and the AAAPT resulted in push to a new direction of applications of the code. Beam-target mechanism incorporated with realistic simulation of yield resulted in re-examination of neutron scaling laws. Plasma self-absorption and taper features completed. Technique to find I_{pinch} from measured I_{total} waveform published. A new effect of focus pinch current limitation was uncovered. All these activities resulted in the formation of Institute for Plasma Focus Studies to encourage correct usage and innovative applications of the Lee model code. Further development of the code is continuously undertaken. List of papers.

Are the results any good?

Are there any indications that our computed results are anywhere near the actual results that may be measured on the device in actual operation?

NOT if we just guess the model parameters f_m, f_c, f_{mr}, f_{cr};. Then the results are just hypothetical; although with experience we may assign some reasonable values of the model parameters for the particular machine in its particular operating conditions. And the results may be useful for planning or designing purposes.

How do we make the results realistic?

The standard practice is to **fit the computed total current waveform to an experimentally measured total current waveform.**

From experience it is known that the current trace of the focus is one of the best indicators of gross performance. The axial and radial phase dynamics and the crucial energy transfer into the focus pinch are among the important information that is quickly apparent from the current trace.

The exact time profile of the total current trace is governed by the **bank parameters** namely capacitance C_o, external, or static inductance L_o and circuit resistance r_o, by the focus **tube geometry** namely electrode radii, outer 'b' and inner anode 'a', and the anode length 'z_o'; and on the **operational parameters** which are the charging voltage V_o and the fill pressure P_o and the fill gas. It also depends on the fraction of mass swept-up and the fraction of sheath current and the variation of these fractions through the axial and radial phases. These parameters determine the axial and radial dynamics, specifically the axial and radial speeds which in turn affect the profile and magnitudes of the discharge current. The detailed profile of the discharge current during the pinch phase will also reflect the joule heating and radiative yields. At the end of the pinch phase the total current profile will also reflect the sudden transition of the current flow from a constricted pinch to a large column flow. Thus the discharge current powers all the

dynamic, electrodynamic, thermodynamic and radiation processes in the various phases of the plasma focus. Conversely all the dynamic, electrodynamic, thermodynamic and radiation processes in the various phases of the plasma focus affect the discharge current. It is then no exaggeration to say that **the discharge current waveform contains information on all the dynamic, electrodynamic, thermodynamic and radiation processes that occurs in the various phases of the plasma focus**.

Our standard practice for any existing plasma focus is to obtain a measured current trace. Then we fit the computed current trace to the measured current trace. The fitting process involves adjusting the model parameters f_m, f_c, f_{mr}, f_{cr} one by one, or in combination until the computed current waveform fits the measured current waveform.

Once this fitting is done our experience is that the other computed properties including dynamics, energy distributions and radiation are all realistic.

Fitting computed current trace to experimental current trace of existing machine:

The main model parameters are the tube current flow factor CURRF (known to be 0.7 for most machines) and the mass swept-up factor (MASSF, for axial & MASSFR, for radial). First try model parameters are suggested in a table towards the right of the worksheet. These could be tried, but may be adjusted so that the time of focus, and the radial inward shock transit time, fit the experimentally observed times for each machine. The computed current trace is compared with the experimental current trace.

Features for comparison include current risetime and rising shape, peak current, current 'roll off' and dip, both shape and amplitude. Absolute values should be compared. Our experience with a number of machines shows that the fit is usually very good, occasionally almost exact..
The machine parameters and operating conditions should already have been determined and inputted into the active sheet. The model parameters are then adjusted, one by one, or in combination until best fit is obtained between the computed current trace and the experimental current trace.

First step is fitting the axial phase. This involves variation of f_m and f_c whilst observing the changes that appear on the resulting computed I_{total} trace in respect to the **risetime, rising shape and I_{peak}**; and how these features compare with the corresponding features of the measured I_{total} trace. During this fitting an increase in f_c increases axial speed which increases dynamic resistance, thus lowering current magnitude on the rising slope. The greater rate of increase of tube inductance flattens out the rising slope. A decrease in f_m has almost the same effect. However a change in f_c has an additional subtle effect of changing the relative effect of the tube inductance. This means that increasing the speed by a certain amount by increasing f_c, then reducing it by exactly the same amount by a corresponding increase in f_m will not bring the I_{total} shape and magnitude back to the shape and value before either change is made. Thus one has to get each of f_m and f_c separately correct to get both the current shape and magnitude correct in the rising current profile.

Second step is fitting of the radial phases. We need particularly to understand the transition from the axial to the radial phase. For a plasma focus to work well, it is usually operated with a speed such that its axial run-down time is about equal to the risetime of the circuit with the device short-circuited across its back-wall. With the focus tube connected, the current risetime will be larger. At the same time the current trace is flattened out. In most cases this increased risetime will be cut short by the start of the radial phase. As this phase starts the current trace starts to roll over, at first imperceptibly, then clearly dipping and then dips sharply as the focus dynamics enters the severe pinch phase which absorbs a significant portion of the energy from the driving magnetic field. Thus, the second step in the fitting consists of adjusting f_{mr} and f_{cr} so that the computed current roll-over and the dip agree in shape, slope and extent of dip with the measured waveform.

[The rest of the notes may be left to be read in conjunction with the work of Part 3.]

Besides the model parameters, sometimes (when all else fails in the fitting process) the inductance (as published or given by the experimenters) needs to be adjusted. Very commonly the inductance L_o may be given as the short circuit bank inductance whereas it should be the 'static' inductance of the plasma focus; ie the inductance of the PF before the current sheet moves.

Adjustment to L_o is indicated when the computed current rise slope differs significantly from the measured slope. (adjustment to C_o will also

affect the current slope, but the value of C_o is usually more reliably given than that of L_o).

Usually also the value of stray resistance r_o needs to be guessed at as few experimenters determine this carefully if at all. We usually start with the value of r_o as 0.1 of $(L_o/C_o)^{0.5}$; and make small adjustment as necessary; noting that capacitor banks are such that the ratio of RESF= $r_o / (L_o/C_o)^{0.5}$ seldom goes below 0.05.

Sometimes, especially for PF's using very low values of C_o, it may also be necessary (when all else fails) to adjust the value of C_o (for sub-uF capacitor banks, the closely spaced connecting parallel plates and parallel connecting cables may actually significantly change the value of C_o).

In cases where there is very good fit in current profiles but the absolute values of currents don't match, it has been reasonable to suspect that the calibration constant for the current profile has been given wrongly by the experimenter. Calibration errors can be ascertained by checking the quantity of charge that has flowed out of the capacitor when the voltage across it has dropped to zero. If this quantity differs significantly from $(1/2)C_oV_o^2$; then the suspicion of calibration error is confirmed. Actually this checking is already implicit in the model.

In adjusting r_o we note that an increase of r_o lowers the current trace at all points proportionately. In adjusting L_o we note that increasing L_o lowers the slope of the rising current. When all values are properly adjusted and when f_m and f_c are correctly fitted, the measured rising profile of the computed I_{total}, usually up to the peak value I_{peak}, is found to fit the measured rising profile well in both shape and magnitude.

Two other points need to be noted[6,7]. The measured I_{total} profile usually has a starting portion which seems to rise more slowly than the computed trace. This is due to the switching process during which, until fully switched, the spark gap presents additional resistance. It could also be compounded by the lift-off delay[22]. Practically this effect is compensated by shifting the whole computed trace forward in time, usually by a small amount around 50ns. A related note is that z_o may need to be reduced to account for the shape of the back-wall insulator.

A final remark in response to the general observation that the measured slope of the current dip towards the end of the radial phases is almost always steeper than can be reasonably fitted. This is indeed the case. All adjustments e.g. to L_o, C_o and r_o do not have the necessary short-time influence on this feature of the current trace. To steepen the dip slope the best we could do is to either decrease f_{mr} or increase f_{cr}; however either of these

adjustments also tend to increase the computed depth of the dip; which often is already excessive. Moreover there are usually small but significant 'bouncing' features towards and beyond the bottom of the measured current dip. These features are not modeled. So the fitting has to accept the best compromise to achieve the 'best' fit. I tend to attribute this as a limitation of the model at this stage of its development.

Moreover this method of fitting the computed current to the measured current obviously depends on the actual plasma focus machine performing in accordance to the main features of the model. The plasma focus operated in the so-called 'neutron optimised' mode appears to be most suited for this model. For gases other than Deuterium, perhaps we can also identify range/modes of operations suitable for simulation with this model; e.g. a plasma focus in Neon operated to optimize SXR yield with a temperature around 100-400eV appears also to be very suited to this model code.

On the other hand, unoptimised machines, for example, may have axial phase current sheet so much fragmented that the axial phase model parameters just cannot be stretched for the model to fit the experiment. Or as another example, a plasma focus may be operated to optimize ion or electron beams; in which case conditions are manipulated for the instabilities to be so much enhanced that the radial model parameters cannot be stretched to simulate these effects. Such situations and range of operation may be outside the scope of this mode.

Despite these limitations, our experience show that the model may be used to compute plasma conditions and neutron and SXR yields with reasonable agreement over an unprecedented range of experiments, from sub-kJ PF400 (Chile) to low kJ NX2 (Singapore) and UNU/ICTP PFF (Network countries) all the way to the MJ PF1000.

IPFS

knowledge should be freely accessible to all

Institute for Plasma Focus Studies

Internet Workshop on Numerical Plasma Focus Experiments

(Supplementary Notes SP3 for Module 3)

[in part extracted from file 2Theory.pdf from:
http://www.intimal.edu.my/school/fas/UFLF/] and from various papers

Radiation Terms

The Bremsstrahlung loss term may be written as:

$$\frac{dQ_B}{dt} = -1.6x10^{-40} N_i^2 \left(\pi r_p^2\right) z_f T^{1/2} z^3$$

$$N_o = 6x10^{26} \frac{\rho_o}{M}; \quad N_i = N_o f_{mr} \left(\frac{a}{r_p}\right)^2$$

Recombination loss term is written as:

$$\frac{dQ_{rec}}{dt} = -5.92x10^{-35} N_i^2 Z^5 \left(\pi r_p^2\right) z_f / T^{0.5}$$

The line loss term is written as:

$$\frac{dQ_L}{dt} = -4.6x10^{-31} N_i^2 Z Z_n^4 \left(\pi r_p^2\right) z_f / T$$

$$and \ \frac{dQ}{dt} = \frac{dQ_J}{dt} + \frac{dQ_B}{dt} + \frac{dQ_L}{dt} + \frac{dQ_{rec}}{dt}$$

where dQ/dt is the total power gain/loss of the plasma column.

By this coupling, if, for example, the radiation loss $\left(\frac{dQ_B}{dt} + \frac{dQ_L}{dt}\right)$ is severe, this would lead to a large value of $\frac{dr_p}{dt}$ inwards. In the extreme case, this leads to radiation collapse, with r_p going rapidly to zero, or to such small values that the plasma becomes opaque to the outgoing radiation, thus stopping the radiation loss.

This radiation collapse occurs at a critical current of 1.6 MA (the Pease-Braginski current) for deuterium. For gases such as Neon or Argon, because of intense line radiation, the critical current is reduced to even below 100kA, depending on the plasma temperature.

Plasma Self Absorption and transition from volumetric emission to surface emission

Plasma self absorption and volumetric (emission described above) to surface emission of the pinch column have been implemented in the following manner.

The photonic excitation number (see File 3 Appendix by N A D Khattak) is written as follows:
$M = 1.66 \times 10^{-15} r_p Z_n^{0.5} n_i / (Z T^{1.5})$ with T in eV, rest in SI units
The volumetric plasma self-absorption correction factor A is obtained in the following manner:
$A_1 = (1 + 10^{-14} n_i Z) / (T^{3.5}))$
$A_2 = 1 / AB_1$
$A = A_2^{(1 + M)}$

Transition from volumetric to surface emission occurs when the absorption correction factor goes from 1 (no absorption) down to 1/e (e=2.718) when the emission becomes surface-like given by the expression:

$$\frac{dQ}{dt} = -const x Z_n^{3.5} Z^{0.5} \left(r_p\right) z_f T^4$$

where the constant *const* is taken as 4.62×10^{-16} to conform with numerical experimental observations that this value enables the smoothest transition, in general, in terms of power values from volumetric to surface emission.

Where necessary another fine adjustment is made at the transition point adjusting the constant so that the surface emission power becomes the same value as the absorption corrected volumetric emission power at the transition point. Beyond the transition point (with A less than 1/e) radiation emission power is taken to be the surface emission power.

Neutron Yield

http://www.intimal.edu.my/school/fas/UFLF/
Adapted from the following papers (with modifications for erratum)

Pinch current limitation effect in plasma focus (This version includes an Erratum)
S. Lee and S. H. Saw, Appl. Phys. Lett. 92, 021503 (2008), DOI:10.1063/1.2827579

Neutron Scaling Laws from Numerical Experiments (This version includes an Erratum)
S Lee and S H Saw, J of Fusion Energy, DOI: 10.1007/s10894-008-9132-7
published first online 20 February 2008 at **http://dx.doi.org/10.1007/s10894-008-9132-7**

Neutron yield is calculated with two components, thermonuclear term and beam-target term.
The thermonuclear term is taken as:
$dY_{th} = 0.5n_i^2 (3.142) r_p^2 z_f <\sigma v>$ (time interval)
where $<\sigma v>$ is the thermalised fusion cross section-velocity product corresponding to the plasma temperature, for the time interval under consideration. The yield Y_{th} is obtained by summing up over all intervals during the focus pinch.

The beam-target term is derived using the following phenomenological beam-target neutron generating mechanism[17], incorporated in the present RADPFV5.13. A beam of fast deuteron ions is produced by diode action in a thin layer close to the anode, with plasma disruptions generating the necessary high voltages. The beam interacts with the hot dense plasma of the focus pinch column to produce the fusion neutrons. In this modeling each factor contributing to the yield is estimated as a proportional quantity and the yield is obtained as an expression with proportionality constant. The yield is then calibrated against a known experimental point.

The beam-target yield is written in the form: $Y_{b-t} \sim n_b n_i (r_p^2 z_p) (\sigma v_b) \tau$
where n_b is the number of beam ions per unit plasma volume, n_i is the ion density, r_p is the radius of the plasma pinch with length z_p, σ the cross-section of the D-D fusion reaction, n- branch[18], v_b the beam ion speed and τ is the beam-target interaction time assumed proportional to the confinement time of the plasma column.

Total beam energy is estimated[17] as proportional to $L_p I_{pinch}^2$, a measure of the pinch inductance energy, L_p being the focus pinch inductance. Thus the number of beam ions is $N_b \sim L_p I_{pinch}^2 / v_b^2$ and n_b is N_b divided by the focus pinch volume. Note that $L_p \sim \ln(b/r_p) z_p$, that[4] $\tau \sim r_p \sim z_p$, and that $v_b \sim U^{1/2}$ where U is the disruption-caused diode voltage[17]. Here 'b' is the cathode radius. We also assume reasonably that U is proportional to V_{max}, the maximum voltage induced by the current sheet collapsing radially towards the axis.

Hence we derive: $$\mathbf{Y_{b-t} = C_n n_i I_{pinch}^2 z_p^2 ((\ln b/r_p)) \sigma / V_{max}^{1/2}} \qquad (1)$$

where I_{pinch} is the current flowing through the pinch at start of the slow compression phase; r_p and z_p are the pinch dimensions at end of that phase. Here C_n is a constant which in practice we will calibrate with an experimental point.

The D-D cross-section is highly sensitive to the beam energy so it is necessary to use the appropriate range of beam energy to compute σ. The code computes V_{max} of the order of 20-50 kV. However it is known[17], from experiments that the ion energy responsible for the beam-target neutrons is in the range 50-150keV[17], and for smaller lower-voltage machines the relevant energy [19] could be lower at 30-60keV. Thus to align with experimental observations the D-D cross section σ is reasonably obtained by using beam energy equal to 3 times V_{max}.

A plot of experimentally measured neutron yield Y_n vs I_{pinch} was made combining all available experimental data[2,4,12,13,17,19-22]. This gave a fit of $Y_n = 9 \times 10^{10} I_{pinch}^{3.8}$ for I_{pinch} in the range 0.1-1MA. From this plot a calibration point was chosen at 0.5MA, $Y_n = 7 \times 10^9$ neutrons. The model code[23] RADPFV5.13 was thus calibrated to compute Y_{b-t} which in our model is the same as Y_n.

Notes on **The total current and I_{peak}, the plasma current and I_{pinch}**

Extracted From: **Computing Plasma Focus Pinch Current from Total Current Measurement**
S. Lee, S. H. Saw, P. C. K. Lee, R. S. Rawat and H. Schmidt, Appl Phys Letters 92, 111501 (2008) DOI:10.1063/1.2899632

The total current I_{total} waveform in a plasma focus discharge is easily measured using a Rogowski coil. The peak value I_{peak} of this trace is commonly taken as a measure of the drive efficacy and is often used to scale the yield performance of the plasma focus. This is despite the fact that yields should more consistently be scaled to focus pinch current I_{pinch}, since it is I_{pinch} which directly powers the emission processes. The reason many researchers use I_{peak} instead of I_{pinch} for scaling is simply that while I_{peak} is easily measured, I_{pinch}, which is the value of the plasma sheath current Ip at time of pinch, is very difficult to measure even in large devices where it is possible to place magnetic probes near the pinch. This measurement is also inaccurate and perturbs the pinch. In a small device, there is no space for such a measurement.

The relationship between $_{Ipinch}$ and I_{peak} is not simple and has only been recently elaborated. It primarily depends on the value of the static inductance L_0 compared to the dynamic inductances of the plasma focus. As L_0 is reduced, the ratio I_{pinch} / I_{peak} drops. Thus, yield laws scaled to I_{peak} will not consistently apply when comparing two devices with all parameters equal but differing significantly in L_0. Better consistency is achieved when yield laws are scaled to I_{pinch}. In this paper, we propose a numerical method to consistently

Distinguishing the I_{total} waveform from the I_p waveform

A measured trace of I_{total} is commonly obtained with a Rogowski coil wrapped around the plasma focus flange through which is fed I_{total} discharged from the capacitor bank between the coaxial electrodes across the back wall. A part of I_{total}, being the plasma sheath current I_p, lifts off the back-wall insulator and drives a shock wave axially down the coaxial space. We denote f_c as the current fraction I_p/I_{total} for the axial phase and f_{cr} for the radial phases. In modeling it is found that a reasonable value for initial trial for f_c is 0.7 with a similar first trial value for f_{cr}. However in a DPF78 experiment f_c was found to vary from 0 at the start of the axial phase rising rapidly above 0.6 for the rest of the axial phase. In the radial phase f_{cr} was found to stay above 0.6 before dropping to 0.48 at the start of the pinch and then towards 0.4 as the pinch phase progressed. These Stuttgart results confirm a complex relationship between the waveforms of I_{total} and I_p.

The performance of a plasma focus is closely linked to the current I_{pinch} actually participating in the focus pinch phase rather than the total current flowing in the circuit. It is a common practice to take I_{peak} or some representative fraction of it as I_{pinch}. Another practice is to take the value of I_{total} at the time of the pinch as I_{pinch} Whilst in their special cases this practice could be justifiable, the distinction of I_p from I_{total} should generally be clearly made. We emphasize that it should be the value of I_p at the time of pinch which is the relevant value for the purpose of yield scaling. The practice of associating yield

scaling with the total current waveform (i.e. taking I_{peak} or I_{total} at estimated pinch time) would be justifiable if there were a linear relationship between the waveforms of I_{total} and I_p. However as shown by the Stuttgart experiments the actual relationship is a very complex one which we may ascribe to the interplay of the various electro-dynamical processes including the relative values of static inductance L_o, tube inductance and the dynamic resistances which depend on the tube geometry and plasma sheath speeds. This relationship may change from one machine to the next. Whilst these electro-dynamical processes and other relevant ones such as radiation are amenable to modeling there are other machine effects such as back wall restriking (for example due to high induced voltages during the pinch phase) which can almost unpredictably affect the relationship between I_{total} and I_p during the crucial radial phases. Hence it is not only simplistic to discuss scaling in terms of the I_{total} waveform (i.e. taking I_{peak} or the value of I_{total} at the estimated time of pinch) but also inconsistent. One of the most important features of a plasma focus is its neutron production. The well-known neutron yield scaling, with respect to current, based on various compilations of experimental data, is $Y_n \sim I_{pinch}^{x}$ where x is varied in the range 3–5. In a recent paper , numerical experiments using a code was used to derive a scaling with $x = 4.7$. Difficulties in the interpretation of experimental data ranging across big and small plasma focus devices include the assignment of the representative neutron yield Y_n for any specific machine and the assignment of the value of I_{pinch}. In a few larger machines attempts were made to measure I_{pinch} using magnetic probes placed near the pinch region, with uncertainties of 20%. Moreover the probes would have affected the pinching processes. In most other cases related to yield scaling data compilation or interpretation I_{pinch} is simply assigned a value based on the measurement of peak total current I_{peak} or the value of total current at the observed current dip.

The difficulties in distinguishing I_{pinch} from I_{total} are obviated in numerical experiments using the Lee Model [In a typical simulation, the I_{total} trace is computed and fitted to a measured I_{total} trace from the particular focus. Three model parameters for fitting are used: axial mass swept-up factor f_m, current factor f_c and radial mass factor f_{mr}. A fourth model parameter, radial current factor, f_{cr} may also be used. When correctly fitted the computed I_{total} trace agrees with the measured I trace in peak amplitude, rising slope profile and topping profile which characterize the axial phase electro-dynamics. The radial phase characteristics are reflected in the roll-over of the current trace from the flattened top region, and the subsequent current drop or dip. Any machine effects, such as restrikes, current sheath leakage and consequential incomplete mass swept up, not included in the simulation physics is taken care of by the final choice of the model parameters, which are fine-tuned in the feature-by-feature comparison of the computed I_{total} trace with the measured I_{total} trace. Then there is confidence that the computed gross dynamics, temperature, density, radiation, plasma sheath currents, pinch current and neutron yield may also be realistically compared with experimental values.

A note on scaling:

Scaling of yields to say I_{pinch} should be carried out using yields which are at optimum, or at least near optimum. If one indiscriminately uses any data one may end up with

completely trivial or misleading results. For example if a point is used at too high or low pressure (away from the optimum pressure) then there may be zero yield ascribed to values of I_{pinch}.

References

[1] Lee S 1984 *Radiations in Plasmas* ed B McNamara (World Scientific) pp 978–87
Also: S. Lee in *Laser and Plasma Technology*, edited by S. Lee, B. C. Tan, C. S. Wong, & A. C. Chew. World Scientific, Singapore, (1985), pp. 387–420.

[2]S. Lee, T. Y. Tou, S. P. Moo, M. A. Elissa, A. V. Gholap, K. H. Kwek, S. Mulyodrono, A. J. Smith, Suryadi, W. Usala, & M. Zakaullah, Am. J. Phys. **56**, 62 (1988).

[3]T. Y. Tou, S. Lee, & K. H. Kwek, IEEE Trans. Plasma Sci. **17**, 311 (1989).

[4]S. Lee and A. Serban, IEEE Trans. Plasma Sci. **24**, 1101 (1996).

[5]D. E. Potter, Phys. Fluids **14**, 1911 (1971).

[6]M. H. Liu, X. P. Feng, S. V. Springham, and S. Lee, IEEE Trans. Plasma Sci. **26**, 135 (1998).

[7]S. Lee, P. Lee, G. Zhang, X. Feng, V. A. Gribkov, M. Liu, A. Serban, and T. Wong, IEEE Trans. Plasma Sci. **26**, 1119 (1998).

[8]S. Bing, "Plasma dynamics and x-ray emission of the plasma focus," Ph.D. thesis, NIE, (2000) in ICTP Open Access Archive: http://eprints.ictp.it/99/

[9]S. Lee, in http://ckplee.myplace.nie.edu.sg/plasmaphysics/ (2000 & 2007).

[10]S. Lee in ICTP Open Access Archive: http://eprints.ictp.it/85/ (2005).

[11]V. Siahpoush, M. A. Tafreshi, S. Sobhanian, and S. Khorram, Plasma Phys. Controlled Fusion **47**, 1065 (2005).

[12]S. Lee, Twelve Years of UNU/ICTP PFF-A Review (1998) IC, 98 (231); A.Salam ICTP, Miramare, Trieste (in ICTP OAA: http://eprints.ictp.it/31/).

[13]L. Soto, P. Silva, J. Moreno, G. Silvester, M. Zambra, C. Pavez, L. Altamirano, H. Bruzzone, M. Barbaglia, Y. Sidelnikov, and W. Kies, Braz. J. Phys. **34**, 1814 (2004).

[14]H. Acuna, F. Castillo, J. Herrera, and A. Postal, International Conference on Plasma Sci, 3–5 June 1996 (unpublished), p. 127.

[15]C. Moreno, V. Raspa, L. Sigaut,& R. Vieytes, Appl. Phys. Lett. **89**, 15 (2006).

[16]D. Wong, P. Lee, T. Zhang, A. Patran, T. L. Tan, R. S. Rawat, and S. Lee, Plasma Sources Sci. Technol. **16**, 116 (2007).

[17]V A Gribkov, A Banaszak, B Bienkowska, A V Dubrovsky, I Ivanova-Stanik, L Jakubowski, L Karpinski, R A Miklaszewski, M Paduch, M J Sadowski, M Scholz, A. Szydlowski, and K. Tomaszewski, J. Phys. D **40**, 3592 (2007).

[18]J. D. Huba, 2006 Plasma Formulary, p. 44. http://wwwppd.nrl.navy.mil/nrlformulary/NRL_FORMULARY_07.pdf

[19]S. V. Springham, S. Lee, and M. S. Rafique, Plasma Phys. Controlled Fusion 42, 1023 (2000).

[20]W. Kies, in Laser and Plasma Technology, Proceedings of Second Tropical College, edited by S. Lee, B. C. Tan, C. S. Wong, A. C. Chew, K. S. Low, H. Ahmad, and Y. H. Chen World Scientific, Singapore, (1988), pp. 86–137.

[21]H. Herold, in Laser and Plasma Technology, Proceedings of Third Tropical College, edited by C. S. Wong, S. Lee, B. C. Tan, A. C. Chew, K. S. Low, and S. P. Moo World Scientific, Singapore, (1990), pp. 21–45.

[22]A. Patran, R. S. Rawat, J. M. Koh, S. V. Springham, T. L. Tan, P. Lee, & S. Lee, 31st EPS Conf on Plasma Phys London, (2004), Vol. 286, p. 4.213.

[23]S Lee **Radiative Dense Plasma Focus Computation Package (2008)** RADPF: http://www.intimal.edu.my/school/fas/UFLF/

Reference to this course and the Lee model code should be given according to the following format:

Lee S. Radiative Dense Plasma Focus Computation Package (2008): RADPF
www.plasmafocus.net www.intimal.edu.my/school/fas/UFLF/

Theoretical Basis: Plasma Focus Model (Radiative)-S Lee Model

http://www.intimal.edu.my/school/fas/UFLF/

(This revision, 17 March 2008, conforms to RADPFV5.13.8, including beam-target neutron yield and plasma self-absorption with smooth transition from volumetric to surface emission)

This model has been developed for Mather-type (1) plasma focus machines. It was developed for the 3kJ machine known as the UNU/ICTP PFF (2,3) (United Nations University/International Centre for Theoretical Physics Plasma Focus facility, which now forms an international network.In principal there is no limit to energy storage and electrode configuration, though house-keeping may need to be carried out in extreme cases, in order to keep within efficient ranges e.g. of graph plotting.

For details of the computing package, go back to the introductory section.
http://www.intimal.edu.my/school/fas/UFLF/

The model has been used for various applications, for example, in the design of a cascading plasma focus (Ref 4); and for estimating soft x-ray yield (Ref 5) for the purpose of developing a SXR source for microelectronics lithography (Ref 6); and recently in uncovering a pinch current limitation effect (Ref 7, 2008) , throwing new light on neutron scaling laws (Ref 8, 2008) and as an experimental technique (Ref 9, 2008) to compute focus pinch current from a measured discharge current waveform.

The 5-phase model is described in some detail in the following sections:

1 Axial Phase (snow-plow model)

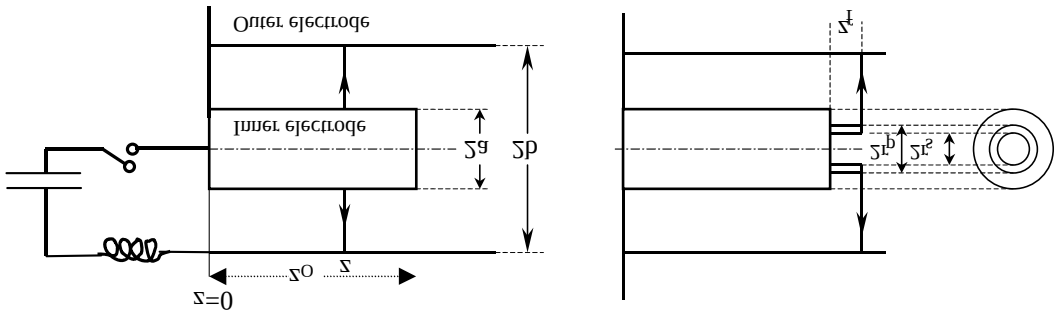

Fig 1 (a) Fig 1 (b)

Rate of change of momentum at current sheath, position z, is

$$\frac{d(mv)}{dt} = \frac{d}{dt}\left(\left[\rho_o \pi (b^2 - a^2) z\right] f_m \frac{dz}{dt}\right) = \rho_o \pi \left(c^2 - 1\right) a^2 \mathrm{f}_m \frac{d}{dt}\left(z \frac{dz}{dt}\right)$$

Magnetic force on current sheath is

$$F = \int_a^b \left[\left(\frac{\mu I f_c}{2\pi r}\right)^2 /(2\mu)\right] 2\pi r dr = \frac{\mu \mathrm{f}_c^{\,2}}{4\pi} \ln(c) I^2$$

f_m = fraction of mass swept down the tube in the axial direction
f_c = fraction of current flowing in piston

Equation of motion:

$$\rho_o \pi (c^2 - 1) a^2 \mathrm{f}_\mathrm{m} \frac{d}{dt}\left(z \frac{dz}{dt}\right) = \frac{\mu \mathrm{f} c^2}{4\pi} (\ln c) I^2$$

$$\therefore \frac{d^2 z}{dt^2} = \left[\frac{\mathrm{f}_\mathrm{c}^{\,2}}{f_m} \frac{\mu (\ln c)}{4\pi^2 \rho_o (c^2 - 1)} \left(\frac{I}{a}\right)^2 - \left(\frac{dz}{dt}\right)^2\right] / z \qquad \text{-- (I)}$$

Circuit (current) Equation

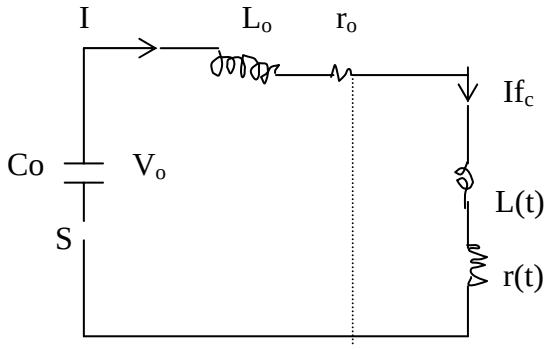

Fig 2 Circuit schematic

Ignore r(t), plasma resistance. This is the approximation which is generally used for electromagnetic drive.

$$\frac{d}{dt}\left[(L_o + Lf_c)I\right] + r_o I = V_o - \int \frac{Idt}{C_o}$$

$$(L_o + Lf_c)\frac{dI}{dt} + If_c \frac{dL}{dt} + r_o I = V_o - \int \frac{Idt}{C_o} \qquad \text{-- (II)}$$

$$\frac{dI}{dt} = \left[V_o - \frac{\int Idt}{C_o} - r_o I - If_c \frac{\mu}{2\pi}(\ln c)\frac{dz}{dt}\right] \Big/ \left[L_o + \frac{f_c \mu}{2\pi}(\ln c)z\right]$$

Equations (I) and II) are the generating equations of the model.
They contain the physics built into the model.

They are coupled equations.

The equation of motion is affected by the electric current I.

The circuit equation is affected by the current sheath motion dz/dt and position z.

Normalise the equations to obtain scaling parameters

Replace variables t, z, I by non-dimensionalised quantities as follows:

$$\tau = t/t_o, \quad \varsigma = z/z_o, \quad \iota = I/I_o$$

where the normalising quantities t_o, I_o and Z_o are carefully chosen to be relevant, characteristic, convenient quantities, reflecting the physics of the problem.

Choices:

z_o is the length of the anode,

t_o is $\sqrt{L_o C_o}$ (noting that $2\pi\sqrt{L_o C_o}$ is the cycle time of L_o-C_o discharge circuit)

I_o is V_o/Z_o where $Z_o = \sqrt{L_o/C_o}$ is the surge impedance (noting that I_o is the peak current of the L_o-C_o discharge circuit with capacitor C_o charged initially to V_o.)
Normalising, we have:

Equation of motion:

$$\frac{z_o}{t_o^2}\frac{d^2\zeta}{d\tau^2} = \left[\frac{f_c^2}{f_m}\frac{\mu \ln c}{4\pi^2\rho_o(c^2-1)}\left(\frac{I_o}{a}\right)^2 \iota^2 - \frac{z_o^2}{t_o^2}\left(\frac{d\zeta}{d\tau}\right)^2\right] \Big/ \zeta z_o$$

$$\frac{d^2\zeta}{d\tau^2} = \left[\frac{f_c^2}{f_m}\frac{\mu \ln c}{4\pi^2\rho_o(c^2-1)}\left(\frac{I_o}{a}\right)^2 \frac{t_o^2}{z_o^2}\iota^2 - \left(\frac{d\zeta}{d\tau}\right)^2\right] \Big/ \zeta$$

which we write as

$$\frac{d^2\zeta}{d\tau^2} = \frac{\left[\alpha^2\iota^2 - \left(\frac{d\zeta}{d\tau}\right)^2\right]}{\zeta} \qquad \text{-- (I.1)}$$

Obtain first scaling parameter:

We note, by inspection,

$\alpha^2 = t_o^2 / \left\{\left[z_o^2/(I_o/a)^2\right](f_m/f_c^2)\left[4\pi^2\rho_o(c^2-1)/\mu \ln c\right]\right\}$, which we thus define in this manner.

By inspection of equation (I.1), we note α is dimensionless.

Hence since t_o has the dimension of time we may define a time value t_a where

$$t_a = \left[\frac{4\pi^2(c^2-1)}{\mu \ln c}\right]^{1/2} \frac{\sqrt{f_m}}{f_c}\frac{z_o}{(I_o/a)/\sqrt{\rho}}$$

identifying this quantity as the characteristic axial transit time of the CS down the anode axial phase.

We may then think of α as:

$\alpha = (t_o/t_a)$ – scaling parameter.

ratio of characteristic electrical discharge time to characteristic axial transit time.

We may further identify a characteristic axial transit speed $V_a = z_o/t_a$

$$v_a = \left[\frac{\mu \ln c}{4\pi^2(c^2-1)}\right]^{1/2} \frac{f_c}{\sqrt{f_m}}\frac{(I_o/a)}{\sqrt{\rho}}$$

The quantity $\left(I_o/a\right)/\sqrt{\rho}$ is the S (speed or drive) factor of electromagnetically driven devices, focus, pinches etc.

Normalising the circuit (current) Equation, we have:

$$\frac{I_o}{t_o}\frac{d\imath}{d\tau}=\left[v_o-\frac{I_o t_o}{c_o}\int \imath d\tau - r_o I_o \imath - f_c \frac{\mu}{2\pi 1}(\ln c) I_o \frac{z_o}{t_o}\imath\frac{d\zeta}{d\tau}\right]/\left[L_o+\frac{\mathrm{f}_c\mu}{2\pi}(\ln c) z_o \zeta\right]$$

and substituting in $I_o = V_o/\sqrt{L_o/C_o}, t_o=\sqrt{L_o C_o},$ we have

$$\frac{d\imath}{d\tau}=\left[1-\int \imath d\tau - \mathrm{f_c}\left[\left(\frac{\mu}{2\pi}(\ln c) z_o\right)/L_o-(r_o/Z_{o)}\right]\imath\frac{d\zeta}{d\tau}\right]\left[1+\mathrm{f_c}\left[\frac{\mu}{2\pi}(\ln c) z_o\right]\zeta/L_o\right]$$

write: $\frac{d\imath}{d\tau}=\left(1-\int \imath d\tau-\beta\imath\frac{d\zeta}{d\tau}-\delta\imath\right)/(1+\beta\zeta)$ -- (II.1)

Second scaling parameter

We note $L_a=\frac{\mathrm{f_c}\mu}{2\pi}(\ln c) z_o$ is the inductance of the axial phase when CS reaches the end z = z_o.

Hence $\beta=\frac{L_a}{L_o}$ is the ratio of load to source inductance and since the device is electromagnetic, the electrodynamics is determined strongly by this scaling parameter.

The third scaling parameter $\delta = r_o/Z_o$ is the ratio of circuit stray resistance to surge impedance. This acts as a damping effect on the current.

(I.1) and (II.1) are the Generating Equations that may be integrated step-by-step.

Calculate voltage across input terminals of focus tube:

$$V=\frac{d}{dt}(LI\mathrm{f}_c)=\mathrm{f_c} I\frac{dL}{dt}+\mathrm{f_c}L\frac{dI}{dt}\quad where\quad L=\frac{\mu}{2\pi}(l_n c)$$ - (II.10)

Normalized form $\upsilon=\frac{V}{V_o}=\beta\imath\frac{d\zeta}{d\tau}+\beta\zeta\frac{d_c}{d\tau}$ - (II.11)

Integration

Define initial conditions:

$$\tau=0,\quad \frac{d\zeta}{d\tau}=0,\quad \zeta=0,\quad \imath=0,\quad \int \imath d\tau=0,\quad \frac{d\imath}{d\tau}=1,\quad \frac{d^2\zeta}{d\tau^2}=\alpha\sqrt{2/3}$$

Set time increment: D = 0.001

Increment time: $\tau = \tau + D$

Next step values are computed using the following linear approximations:

$$\frac{d\zeta}{d\tau} = \frac{d\zeta}{d\tau} + \frac{d^2\zeta}{d\tau^2} D$$

$$\zeta = \zeta + \frac{d\zeta}{d\tau} D$$

$$\imath = \imath + \frac{d\imath}{d\tau} D$$

$$\int \imath d\tau = \int \imath d\tau + \imath D$$

Use new values of $\frac{d\zeta}{d\tau}, \zeta, \imath \text{ and } \int \imath d\tau$ to calculate new generating values of $\frac{d\imath}{d\tau}$ and $\frac{d^2\zeta}{d\tau^2}$ using generating equs (I.1) and (II.1).

Increment time again and repeat calculations of next step values and new generating values.

Continue procedure until $\zeta = 1$.

Then go on to radial phase inward shock computations.

2 Radial Inward Shock Phase (Slug model)

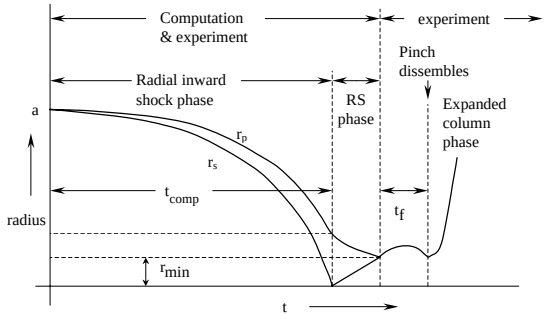

Fig 3. Schematic of radial phases

The snowplow model is used for axial phase just to obtain axial trajectory and speed (from which temperature may be deduced) and to obtain reasonable current profile. As the CS is assumed to be infinitesmally thin, no information of density is contained in the physics of the equation of motion, although an estimate of density may be obtained by invoking additional mechanisms e.g. using shock wave theory.

In the radial phase however, a snowplow model (with an infinitesmally thin CS) would eventually (in the integration) lead to all current flowing at r = 0, with infinite inductance and density.

We thus replace the snow plow model by a slug model . In this model, the magnetic pressure drives a shock wave ahead of it, creating a space for the magnetic piston (CS) to move into.

The speed of the inward radial shock front (see Fig 1b)is determined by the magnetic pressure (which depends on the drive current value and CS position r_p).

The speed of the magnetic piston (CS) is determined by the first law of thermodynamics applied to the effective increase in volume between SF and CS, created by the incremental motion of the SF.

The compression is treated as an elongating pinch.

Four generating equations are needed to describe the motion of (a) SF, (b) CS (c) pinch elongation and the electric current (d); to integrate for the four variables r_s, $r_{p,}$ z_f & I.

Motion of Shock Front:

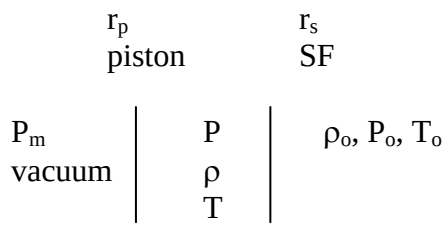

From Shock Wave theory, shock pressure $P = \frac{2}{\gamma+1}\rho_o v_s^{\,2}$ where shock speed v_s into ambient gas ρ_o causes the pressure of the shocked gas (just behind the shock front) to rise to value P.

If we assume that this pressure is uniform from the SF to the CS (infinite acoustic [small disturbance] speed approximation) then across the piston, we may apply $P = P_m$ where

$$P_m = \left(\mu I f_c / 2\pi r_p\right)^2 / 2\mu$$

Thus: $v_s^2 = \frac{\mu(I\mathrm{f_c})^2}{8\pi^2 r_p} x \frac{\gamma+1}{2\rho_o \mathrm{f_{mr}}}$

where I is the circuit current and Ifc is the current flowing in the cylindrical CS, taken as the same f_c as in the axial phase, and $\rho_o f_{mr}$ is the effective mass density swept into the radial slug; where f_{mr} is a different (generally larger) factor than f_m of the axial phase.

Thus $\frac{dr_s}{dt} = -\left[\frac{\mu(\gamma+1)}{\rho_o}\right]^{1/2} \frac{\mathrm{f_c}}{\sqrt{\mathrm{f_{mr}}}} \frac{I}{4\pi r_p}$ -- (III)

Elongation speed of CS (open-ended at both ends)

The radial compression is open at one end. Hence an axial shock is propagated in the z-direction, towards the downstream anode axis. We take z_f as the position of the axial CS (rather than the SF). The pressure driving the axial shock is the same as the pressure driving the inward radial shock. Thus the axial shock speed is the same as the radial shock speed. The CS speed is slower, from shock wave theory, by an approximate factor of $2/(\gamma+1)$. Thus the axial elongation speed of the CS is:

$$\frac{dz_f}{dt} = -\left(\frac{2}{\gamma+1}\right)\frac{dr_s}{dt} \qquad \text{-- (IV)}$$

In this modelling we treat the elongation in a very approximate fashion, as its effect on the compressing column is relatively secondary. The main mechanism controlling the state of the plasma column is the radial compression. The radial CS (piston) speed is hence treated with more care as follows:

Radial piston motion

We inquire:

For an incremental motion, dr_s, of the shock front, at a driving current I, what is the relationship between plasma slug pressure P and plasma slug volume V?

We assume an adiabatic relationship (7) (infinite small disturbance speed – for which we will apply a correction subsequently) to a <u>fixed mass of gas</u> in the slug during the incremental motion dr_s. We have

PV^{γ} = constant or

$$\frac{\gamma dV}{v} + \frac{dP}{P} = 0$$

where slug pressure $P \sim v_s^2$

so $\frac{dP}{P} = \frac{2dv_s}{v_s}$

but $v_s \sim \frac{I}{r_p}$ (see section on Motion of Shock Front, above)

so $\frac{dP}{P} = 2\left(\frac{dI}{I} - \frac{dr_p}{r_p}\right)$

Now slug volume $V = \pi (r_p^2 - r_s^2) z_f$

and at first sight $dV = 2\pi (r_p dr_p - r_s dr_s) z_f + \pi (r_p^2 - r_s^2) dz_f$ – not correct!

But here we note that although the motion of the piston dr_p does not change the mass of gas in the slug, the motion of the shock front, dr_s, <u>does</u> sweep in an amount of ambient gas.

This amount swept in is equal to the ambient gas swept through by the shock front in its motion dr_s. This swept-up gas is compressed by a ratio $(\gamma+1)/(\gamma-1)$ and will occupy part of the increase in volume dV.
The actual increase in volume available to the original mass of gas in volume V does not correspond to increment dr_s but to an effective (reduced) increment drs $(2/(\gamma+1))$. (Note γ is specific heat ratio of

the plasma e.g. γ = 5/3 for atomic gas, γ = 7/5 for molecular gas; for strongly ionising argon γ has value closer to 1 e.g. 1.15.)

Thus, the more correct interpretation is:

$$dV = 2\pi\left(r_p dr_p - \frac{2}{\gamma+1} r_s dr_s \right) z_f + \pi\left(r_p{}^2 - r_s^2\right) dz_f$$

Thus we have: $\frac{\gamma dV}{V} = \frac{2\gamma\left(r_p dr_p - \frac{2}{\gamma+1} r_s dr_s \right) z_f + \gamma\left(r_p{}^2 - r_s{}^2\right) dz_f}{z_f\left(r_p^2 - r_s^2\right)}$

and adding together dP/P and γdV/V we have

$$\frac{2\gamma\left(r_p dr_p - \frac{2}{\gamma+1} r_s dr_s \right) z_f + \gamma\left(r_p{}^2 - r_s{}^2\right) dz_f}{z_f\left(r_p{}^2 - r_s{}^s\right)} + 2\frac{dI}{I} - \frac{2dr_p}{r_p} = 0$$

Rearranging and putting dr_p as the subject we have

$$\frac{dr_p}{dt} = \frac{\frac{2}{\gamma+1}\frac{r_s}{r_p}\frac{dr_s}{dt} - \frac{r_p}{\gamma I}\left(1 - \frac{r_s{}^2}{r_p{}^2}\right)\frac{dI}{dt} - \frac{1}{(\gamma+1)}\frac{r_p}{z_f}\left(1 - \frac{r_s{}^2}{r_p{}^2}\right)\frac{dz_f}{dt}}{\frac{\gamma-1}{\gamma} + \frac{1}{\gamma}\frac{r_s{}^2}{r_p{}^2}} \qquad \text{-- (V)}$$

where we are reminded r_p = radial piston position
r_s = radial shock front position
z_f = axial piston position

Circuit Equation during radial phase

The inductance of the focus tube now consists of the full inductance of the axial phase and the inductance of the radially imploding & elongating plasma pinch.

Thus $L = \frac{\mu}{2\pi}(\ln c) z_o + \frac{\mu}{2\pi}\left(\ln\frac{b}{r_p}\right) z_f$ where both z_f and r_p vary with time.

Thus the circuit (current) equation is

$$\left\{ L_o + f_c \frac{\mu}{2\pi}(\ln c) z_o + f_c \frac{\mu}{2\pi}\left(\ln\frac{b}{r_p}\right) z_f \right\}\frac{dI}{dt} + f_c I \frac{\mu}{2\pi}\left(\ln\frac{b}{r_p}\right)\frac{dz_f}{dt} - f_c I \frac{\mu}{2\pi}\frac{z_f}{r_p}\frac{dr_p}{dt} + r_o I$$
$$= V_o - \frac{\int I dt}{C_o}$$

Giving $$\frac{dI}{dt} = V_o - \frac{\int I dt}{C_o} - r_o I - \mathrm{f_c}\frac{\mu}{2\pi}\left(\ln\frac{b}{r_p}\right) I\frac{dz_\mathrm{f}}{dt} + \mathrm{f_c}\frac{\mu}{2\pi}\frac{z_\mathrm{f}}{\mathrm{r_p}} I\frac{dr_p}{dt}$$
$$L_o + \mathrm{f_c}\frac{\mu}{2\pi}(\ln c) z_o + \mathrm{f_c}\frac{\mu}{2\pi}\left(\ln\frac{b}{r_p}\right) z_\mathrm{f}$$
-- (VI)

Generating equations (III), (IV), (V), (VI) form a close set of equations which may be integrated for r_s, r_p, z_f and I.

Normalization

For this phase the following normalization is adopted.

$\tau = t/t_o$, $\iota = I/I_o$ as in axial phase but with $\kappa_s = r_s/a$, $\kappa_p = r_p/a$, $\zeta_f = z_f/a$ ie. distances are normalized to anode radius, instead of anode length.

After normalization we have:

Radial shock speed $$\frac{d\kappa_s}{d\tau} = -\alpha\alpha_1 \iota/\kappa_p$$ -- (III.1)

Axial column elongation speed (both ends of column defined by axial piston)
$$\frac{d\zeta_\mathrm{f}}{\mathrm{d}\tau} = -\frac{2}{\gamma+1}\frac{d\kappa_s}{d\tau}$$
-- (IV.1)

Radial piston speed: $$\frac{d\kappa_p}{d\tau} = \frac{\frac{2}{\gamma+1}\frac{\kappa_s}{\kappa_p}\frac{d\kappa_s}{d\tau} - \frac{\kappa_p}{\gamma\iota}\left(1-\frac{\kappa_s^2}{\kappa_p^{\,2}}\right)\frac{d\iota}{d\tau} - \frac{1}{\gamma+1}\frac{\kappa_p}{\zeta_\mathrm{f}}\left(1-\frac{\kappa_s^2}{\kappa_p^2}\right)\frac{d\zeta_\mathrm{f}}{\mathrm{d}\tau}}{(\gamma-1)/\gamma + (1/\gamma)(\kappa_s^2/\kappa_p^2)}$$ -- (V.1)

current: $$\frac{d\iota}{d\tau} = \frac{1 - \int \iota d\tau + \beta_1\left[\ln(\kappa_p/c)\right]\iota\frac{d\zeta_\mathrm{f}}{\mathrm{d}\tau} + \beta_1\frac{\zeta_\mathrm{f}\iota}{k_p}\frac{d\kappa_p}{d\tau} - \delta\iota}{\left\{1+\beta-(\beta_1)\left[\ln(\kappa_p/c)\right]\zeta_\mathrm{f}\right\}}$$ (VI.1)

where the **scaling parameters** are $\beta_1 = \beta/(\mathrm{Flnc})$, $F = z_o/a$ and
$\alpha_1 = \left[(\gamma+1)(c^2-1)/(4\ln c)\right]^{1/2} F\left[\mathrm{f}_m/\mathrm{f}_{mr}\right]^{1/2}$

Note that whereas we interpret $\alpha = t_o/t_a$, we may interpret $\alpha_1 = t_a/t_r$ where t_r is a characteristic radial transit time.

The **scaling parameter** $\alpha\alpha_1$ may then be interpreted as $\alpha\alpha_1 = \frac{t_o}{t_a} = t_o/t_r$

We note that α_1 the ratio of characteristic axial transit to characteristic radial compression inward shock transit time is essentially a geometrical ratio

$F\left[\left(c^2-1\right)/4\ln c\right]^{1/2} \simeq 20$ (*if* F ≃ 16 and c ≃ 3)
(ie. axial transit time is characteristically 20 times longer than radial shock transit) modified by the thermodynamic term $(\gamma+1)^{1/2}$ and the mass swept up ratio $(f_m / f_{mr})^{1/2}$. Including all 3 factors, the ratio of axial to radial characteristic times is typically 40.

We also note from the scaling parameter $\alpha\alpha_1$ that

$$t_r = \frac{4\pi}{[\,\mu(\gamma+1)\,]^{1/2}} \frac{\sqrt{f_{mr}}}{f_c} \frac{a}{(I_0/a/\sqrt{\rho}}$$

and characteristic speed of inward shock to reach focus axis is:

$$v_r = a/t_r = \frac{[\mu(\gamma+1)]^{1/2}}{4\pi} \frac{f_c}{\sqrt{f_{mr}}} \frac{(I_o/a)}{\sqrt{\rho}}$$

The ratio of characteristic radial and axial speeds is also essentially a geometrical one, modified by thermodynamics. It is $v_r / v_a = \left[\frac{\left(c^2-1\right)(\gamma+1)}{4\ln c}\right]^{1/2}$ with a value typically 2.5.

Note that the radial characteristic speed has the same dependence as the axial transit speed on drive factor $S = (I_o/a)/\sqrt{\rho}$.

Calculate voltage V across PF input terminals

As in the axial phase, the voltage is taken to have only inductive component.

$$V = \frac{d}{dt}(LI)$$

where $L = \frac{\mu}{2\pi}(\ln c) z_o + \frac{\mu}{2\pi}\left(\ln\frac{b}{r_p}\right) z_f$

$$V = \frac{\mu}{2\pi}\left[(\ln c) z_o + \left(\ln\frac{b}{r_p}\right) z_f\right] f_c \frac{dI}{dt} + \frac{\mu}{2\pi}\left[\left(\ln\frac{b}{r_p}\right)\frac{dz_f}{dt} - \frac{z_f}{r_p}\frac{dr_p}{dt}\right] f_c I \qquad \text{- (VI.10)}$$

We may also write in normalised form $\upsilon = V/V_o$
(normalised to initial capacitor voltage V_o)

$$\nu = \left[\beta - \beta_1\left(\ln\frac{\kappa_p}{c}\right)\zeta_f\right]\frac{d\imath}{d\tau} - \beta_1\imath\left[\left(\frac{\zeta_f}{\kappa_p}\right)\frac{d\kappa_p}{d\tau} + \left(\ln\frac{\kappa_p}{c}\right)\frac{d\zeta_f}{d\tau}\right] \qquad \text{- (VI.12)}$$

The generating equations (III.1), (IV.1), (V.1), (VI.1) may now be integrated using the following initial conditions:
τ = the time that axial phase ended
$\kappa_s = 1$
$\kappa_p = 1$
$\zeta_f = 0$ (taken as a small number such as 0.00001 to avoid numerical difficulties for equation V.1)

ι = value of current at the end of the axial phase.
$\int \iota d\tau$ = value of 'flowed charge' at end of axial phase.

The integration (step-by-step) may proceed with the following algorithm: (taking smaller time increment of D = 0.001/100)
Using initial values (above) of κ_s, κ_p, ζ_f and ι
$\frac{d\kappa_s}{d\tau}, \frac{d\zeta_f}{d\tau}, \frac{d\kappa_p}{d\tau}$ *and* $\frac{d\iota}{d\tau}$ are sequentially calculated from generating equation (III.1), (IV.1), (V.1), (VI.1).

$$\kappa_s = \kappa_s + \frac{d\kappa_s}{d\tau} D$$

$$\zeta_f = \zeta_f + \frac{d\zeta_f}{d\tau} D$$

Then sequentially using linear approximation: $\kappa_p = \kappa_p + \frac{d\kappa_p}{d\tau} D$

$$\iota = \iota + \frac{d\iota}{d\tau} D$$

$$\int \iota d\tau = \int \iota d\tau + \iota D$$

Time is then incremented by D, and the next step value of $\frac{d\kappa_s}{d\tau}, \frac{d\zeta_f}{d\tau}, \frac{d\kappa_p}{d\tau}, \frac{d\iota}{d\tau}$ are computed from (III.1), (IV.1), (V.1) and (VI.1), followed by linear approximation for κ_s, ζ_f, κ_ρ, ι and $\int \iota d\tau$.

The sequence is repeated step-by-step until $\kappa_s = 0$.

Correction for finite acoustic (small disturbance) speed.

In the slug model above we assume that the pressure exerted by the magnetic piston (current I, position r_p) is instantaneously felt by the shock front (position r_s). Likewise the shock speed $\frac{dr_s}{dt}$ is instantaneously felt by the piston (CS). This assumption of inifinite small disturbance speed (SDS) is implicit in equations (III) and (V) (or in normalised form (III.1) and (V.1)).

Since the SDS is finite, there is actually a time lapse Δt communicating between the SF and CS. This communication delay has to be incorporated into the model. Otherwise for the PF, the computation will yield too high values of CS and SF speed.

Consider the instant t, SF is at r_s, CS at r_p, value of current is I. SF actually feels the effect of the current not of value I but of a value I_{delay} which flowed at time (t-Δt), with the CS at r_{pdelay}. Similarly the piston 'thinks' the SF speed is not $\frac{dr_s}{dt}$ but $\left(\frac{dr_s}{dt}\right)_{delay}$ at time (t-Δt).

To implement this finite SDS correction we adopt the following procedure:

Calculate the SDS, taken as the acoustic speed.

$$SDS = \left(\frac{\gamma P}{\rho}\right)^{1/2} or \left(\frac{\gamma R_o}{M} D_c T\right)^{1/2}$$

$$or \quad \left(\frac{\gamma D_c kT}{M m_i}\right)^{1/2}$$

where γ = specific heat ratio, M = Molecule Weight,
R_o = universal Gas constant = 8 x 10^3 (SI units)
m_i = mass of proton, k = Boltzmanns constant.
D_c = departure coefficient = DN (1+z)
where Z, here, is the effective charge of the plasma

$Z = \sum_r^J r\alpha_r$, summed over all ionization levels r = 1… J.

DN = dissociation number, e.g. for Deuterium DN = 2, whereas for argon DN = 1.

The temperature T may be computed for the shocked plasma as

$$T = \frac{M}{RoD} \frac{2(\gamma - 1)}{(\gamma + 1)^2} \left(\frac{dr_s}{dt}\right)^2$$

Calculate the communication delay time as
$\Delta T = (r_p - r_s)/SDS$

In our programme using the Microsoft EXCEL VISUAL BASIC, data of the step-by-step integration is stored row-by-row, each step corresponding to one row. Thus the ΔT may be converted to Δ (row number) by using Δ (row number) = ΔT/(timestep increment) this Δ (row number being, of course, rounded off to an integer.

The correction then involves 'looking back' to the relevant row number to extract the corrected values of I_{delay}, r_{pdelay}, $\left(\frac{dr_s}{dt}\right)_{delay}$.

Thus in the actual numerical integration, in equation (III.1), ι and κ_p are replaced by ι_{delay} and κ_{pdelay} and in equation (V.1) $\frac{dk_s}{d\tau}$ is replaced by $\left(\frac{dk_s}{d\tau}\right)_{delay}$

Radial Reflected Shock Phase

When the inward radial shock hits the axis, $\kappa_s = 0$. Thus in the computation, when $\kappa_s \leq 1$ we exit from radial inward shock phase. We start computing the RS phase.

The RS is given a constant speed of 0.3 of on-axis inward radial shock speed.

In this phase computation is carried out in real (SI) units.

Reflected Shock Speed:

$$\frac{dr_r}{dt} = -0.3\left(\frac{dr_s}{dt}\right)_{on-axis}$$

Piston speed:

$$\frac{dr_p}{dt} = \frac{-\frac{r_p}{\gamma I}\left(1-\frac{r_s^{\,2}}{r_p^{\,2}}\right)\frac{dI}{dt} - \frac{1}{\gamma+1}\frac{r_p}{z_f}\left(1-\frac{r_s^{\,2}}{r_p^{\,2}}\right)\frac{dz_f}{dt}}{\frac{\gamma-1}{\gamma}+\frac{1}{\gamma}\frac{r_s^{\,2}}{r_p^{\,2}}}$$

Use the same equation as V except put $\left(\frac{dr_s}{dt}\right) = 0$ and $r_s=0$

Elongation speed:

Use same equation as Eq IV.

$$\frac{dz_f}{dt} = -\left(\frac{2}{\gamma+1}\right)\left(\frac{dr_s}{dt}\right)_{on-axis}$$

Circuit Equation:

Use the same equation as Eq VI.

$$\frac{dI}{dt} = \frac{V_o - \frac{\int I dt}{C_o} - r_o I - f_c\frac{\mu}{2\pi}\left(\ln\frac{b}{r_p}\right) I\frac{dz_f}{dt} + f_c\frac{\mu}{2\pi}\frac{z_f}{r_p} I\frac{dr_p}{dt}}{L_o + f_c\frac{\mu}{2\pi}(\ln c)z_o + f_c\frac{\mu}{2\pi}\left(\ln\frac{b}{r_p}\right)z_f}$$

Continue integrating seamlessly.

Tube Voltage

Use the same equation as Eq (VI.10).

$$V = \frac{\mu}{2\pi}\left[(\ln c)z_o + \left(\ln\frac{b}{r_p}\right)z_f\right] f_c\frac{dI}{dt} + \frac{\mu}{2\pi}\left[\left(\ln\frac{b}{r_p}\right)\frac{dz_f}{dt} - \frac{z_f}{r_p}\frac{dr_p}{dt}\right] f_c I$$

In this phase as the RS (position r_r) moves outwards, the piston (position r_p) continues moving inwards.

Eventually r_r increases until its value reaches the decreasing value of r_p.

We make the assumption that the RS is sufficiently attenuated when it reaches the piston, so that its overpressure is negligible.

In that case, the piston may not be pushed outwards, but will continue to move inwards, although its inward speed may be gradually reduced.

4 Slow Compression Phase

In this phase the piston speed is:

$$\frac{dr_p}{dt} = \frac{\frac{-r_p}{I}\frac{dI}{dt} - \frac{1}{\gamma+1}\frac{r_p}{z_f}\frac{dz_f}{dt} + \frac{4\pi(\gamma-1)}{\mu\gamma z_f}\frac{r_p}{f_c^2 I^2}\frac{dQ}{dt}}{\frac{\gamma-1}{\gamma}} \qquad \text{- (XX)}$$

Here we have included energy loss/gain terms
into the equation of motion.
The plasma gains energy from Joule heating;
and loses energy through Bremsstrahlung & line radiation.
Energy gain term will tend to push the piston outwards.
Energy loss term will have the opposing effect.

Using Spitzer form for resistivity, for the plasma column:

To estimate the temperature, T, we use:

$$\frac{dQ_J}{dt} = RI^2 f_c^2 \quad where \quad R = \frac{1290 Z z_f}{\pi r_p^2 T^{3/2}}$$ where

$$T = \frac{\mu}{8\pi^2 k} I^2 f_c^2 / (DN_o a^2 f_{mr})$$

Radiation Terms

The Bremsstrahlung loss term may be written as:

$$\frac{dQ_B}{dt} = -1.6x10^{-40} N_i^2 \left(\pi r_p^2\right) z_f T^{1/2} z^3$$

$$N_o = 6x10^{26} \frac{\rho_o}{M}; \quad N_i = N_o f_{mr} \left(\frac{a}{r_p}\right)^2$$

Recombination loss term is written as:

$$\frac{dQ_{rec}}{dt} = -5.92x10^{-35} N_i^2 Z^5 \left(\pi r_p^2\right) z_f / T^{0.5}$$

The line loss term is written as:

$$\frac{dQ_L}{dt} = -4.6x10^{-31} N_i^2 Z Z_n^4 \left(\pi r_p^2\right) z_f / T$$

$$and \ \frac{dQ}{dt} = \frac{dQ_J}{dt} + \frac{dQ_B}{dt} + \frac{dQ_L}{dt} + \frac{dQ_{rec}}{dt}$$

where dQ/dt is the total power gain/loss
of the plasma column

By this coupling, if, for example, the radiation loss $\left(\frac{dQ_B}{dt} + \frac{dQ_L}{dt}\right)$ is severe, this would lead to a large value of $\frac{dr_p}{dt}$ inwards. In the extreme case, this leads to radiation collapse, with r_p going rapidly to zero, or to such small values that the plasma becomes opaque to the outgoing radiation, thus stopping the radiation loss.

This radiation collapse occurs at a critical current of 1.6 MA (the Pease-Braginski current) for deuterium. For gases such as Neon or Argon, because of intense line radiation, the critical current is reduced to even below 100kA, depending on the plasma temperature.

Plasma Self Absorption and transition from volumetric emission to surface emission

Plasma self absorption and volumetric (emission described above) to surface emission of the pinch column have been implemented in the following manner.

The photonic excitation number (see File 3 Appendix by N A D Khattak) is written as follows:
$M = 1.66 \times 10^{-15} r_p Z_n^{0.5} n_i / (Z T^{1.5})$ with T in eV, rest in SI units
The volumetric plasma self-absorption correction factor A is obtained in the following manner:
$A_1 = (1 + 10^{-14} n_i Z) / (T^{3.5}))$
$A_2 = 1 / AB_1$
$A = A_2^{(1 + M)}$

Transition from volumetric to surface emission occurs when the absorption correction factor goes from 1 (no absorption) down to 1/e (e=2.718) when the emission becomes surface-like given by the expression:

$$\frac{dQ}{dt} = -constxZ_n^{3.5} Z^{0.5} \left(r_p\right) z_f T^4$$

where the constant *const* is taken as $4.62x10^{-16}$ to conform with numerical experimental observations that this value enables the smoothest transition, in general, in terms of power values from volumetric to surface emission.

Where necessary another fine adjustment is made at the transition point adjusting the constant so that the surface emission power becomes the same value as the absorption corrected volumetric emission power at the transition point. Beyond the transition point (with A less than 1/e) radiation emission power is taken to be the surface emission power.

Neutron Yield

http://www.intimal.edu.my/school/fas/UFLF/
Adapted from the following paper (with modifications for erratum)

Neutron yield is calculated with two components, thermonuclear term and beam-target term.
The thermonuclear term is taken as:
$dY_{th} = 0.5n_i^2(3.142)r_p^2z_f<\sigma v>$(time interval)
Where $<\sigma v>$ is the thermalised fusion cross section-velocity product corresponding to the plasma temperature, for the time interval under consideration. The yield Y_{th} is obtained by summing up over all intervals during the focus pinch.

The beam-target term is derived using the following phenomenological beam-target neutron generating mechanism[17], incorporated in the present RADPFV5.13. A beam of fast deuteron ions is produced by diode action in a thin layer close to the anode, with plasma disruptions generating the necessary high voltages. The beam interacts with the hot dense plasma of the focus pinch column to produce the fusion neutrons. In this modeling each factor contributing to the yield is estimated as a proportional quantity and the yield is obtained as an expression with proportionality constant. The yield is then calibrated against a known experimental point.

The beam-target yield is written in the form: $Y_{b\text{-}t} \sim n_b\, n_i\, (r_p^2 z_p)\, (\sigma\, v_b)\, \tau$
where n_b is the number of beam ions per unit plasma volume, n_i is the ion density, r_p is the radius of the plasma pinch with length z_p, σ the cross-section of the D-D fusion reaction, n- branch[18], v_b the beam ion speed and τ is the beam-target interaction time assumed proportional to the confinement time of the plasma column.

Total beam energy is estimated[17] as proportional to $L_p I_{pinch}^2$, a measure of the pinch inductance energy, L_p being the focus pinch inductance. Thus the number of beam ions is $N_b \sim L_p I_{pinch}^2/v_b^2$ and n_b is N_b divided by the focus pinch volume. Note that $L_p \sim \ln(b/r_p) z_p$, that[4] $\tau \sim r_p \sim z_p$, and that $v_b \sim U^{1/2}$ where U is the disruption-caused diode voltage[17]. Here 'b' is the cathode radius. We also assume reasonably that U is proportional to V_{max}, the maximum voltage induced by the current sheet collapsing radially towards the axis.

Hence we derive: $\mathbf{Y_{b\text{-}t} = C_n\, n_i\, I_{pinch}^2 z_p^2 ((\ln b/r_p))\sigma / V_{max}^{1/2}}$ (1)

where I_{pinch} is the current flowing through the pinch at start of the slow compression phase; r_p and z_p are the pinch dimensions at end of that phase. Here C_n is a constant which in practice we will calibrate with an experimental point.

The D-D cross-section is highly sensitive to the beam energy so it is necessary to use the appropriate range of beam energy to compute σ. The code computes V_{max} of the order of 20-50 kV. However it is known[17], from experiments that the ion energy responsible for the beam-target neutrons is in the range 50-150keV[17], and for smaller lower-voltage machines the relevant energy [19]

could be lower at 30-60keV. Thus to align with experimental observations the D-D cross section σ is reasonably obtained by using beam energy equal to 3 times V_{max}.

A plot of experimentally measured neutron yield Y_n vs I_{pinch} was made combining all available experimental data[2,4,12,13,17,19-22]. This gave a fit of $Y_n=9x10^{10}I_{pinch}^{3.8}$ for I_{pinch} in the range 0.1-1MA. From this plot a calibration point was chosen at 0.5MA, $Y_n=7x10^9$ neutrons. The model code[23] RADPFV5.13 was thus calibrated to compute Y_{b-t} which in our model is the same as Y_n.

Column elongation

Whereas in the radial RS phase we have adopted a 'frozen' elongation speed model, we now allow the elongation to be driven fully by the plasma pressure.

$$\frac{dz_f}{dt}=\left[\frac{\mu(\gamma+1)}{\rho_o}\right]^{1/2}\frac{If_c}{4\pi r_p} \qquad \text{- (XXI)}$$

Circuit current equation

$$\frac{dI}{dt}=\frac{V_o-\frac{\int Idt}{C_o}-\frac{\mu}{2\pi}\left(\ln\frac{b}{r_p}\right)\frac{dz_f}{dt}If_c+\frac{\mu}{2\pi}\frac{z_f}{r_p}\frac{dr_p}{dt}If_c-I(Rf_c+r_o)}{L_o+\frac{\mu}{2\pi}f_c\left((\ln c)z_o+\left(\ln\frac{b}{r_p}\right)z_f\right)} \qquad \text{- (XXII)}$$

Equations (XX), (XXI) and (XXII) are integrated as coupled equations for r_p, z_f and I. At each step the value of $\frac{dQ}{dt}$ is also evaluated as above.

The total energy radiated by Bremsstrahlung (Q_B) and line radiation (Q_L) may also be evaluated.

Voltage across focus terminals

$$V=\frac{\mu f_c}{2\pi}I\left[\left(\ln\frac{b}{r_p}\right)\frac{dz_f}{dt}-\frac{z_f}{r_p}\frac{dr_p}{dt}\right]+\frac{\mu f_c}{2\pi}\left[\left(\ln\frac{b}{r_p}\right)z_f+(\ln C)z_o\right]\frac{dI}{dt}+RI$$

Instability resistance/impedance not included in slow compression phase

From experiments, it is well known that after a brief period (few ns), the quiescent column is rapidly broken up by instabilities. One effect is a huge spike of voltage, partially observed at focus tube terminals. This voltage spike is responsible for driving ion beams (forward direction) and REB (negative direction, up the anode) with energies typically 200keV.

We could model this by including a suitable time varying resistance/impedance into the $\frac{dI}{dt}$ equation; and adjusting this function to suit the observed voltage/beam energy characteristics. There is a complication of this 'annomalous' resistance in our modelling. If we include this resistance also

into the joule heating term in the piston motion Eq (XX), the sudden increase in $\frac{dQ_J}{dt}$ will blow the piston outwards, leading to a huge negative voltage 'spike'; not experienced experimentally. The model may be more realistic if at the moment of introducing the 'annomalous' resistance, the piston motion is 'frozen', or even allowed to continue inwards, as the magnetic field in such 'small Magnetic Reynolds Number' situation will diffuse inwards – no piston blow-out!

The final result of this instability mechanism is the breaking up of the focus pinch into a large expanded current column.

5 Expanded Column Axial Phase

We model the expanded column axial phase (3,4) in the following manner.

In the expanded column phase we assume that the current flows uniformly from anode to cathode in a uniform column having the same radius as the anode and a length of z.

The normalised equations (same normalisation as in axial phase):

Circuit current: $\frac{d\imath}{d\tau} = \frac{1 - \int \imath d\tau - \beta\imath \frac{d\zeta}{d\tau} e - \delta\imath}{1 + \beta + \beta(\zeta - 1)e}$

where $e = \left(\ln c + \frac{1}{z} \right) / \ln c$

Motion: $\frac{d^2\zeta}{d\tau^2} = \frac{\alpha^2 \imath^2 e_1 - h^2 \left(\frac{d\zeta}{d\tau} \right)^2}{1 + h^2(\zeta - 1)}$

where $h = \left[c^2 / (c^2 - 1) \right]^{1/2}$

$e_1 = \left(\ln c + \frac{1}{4} \right) / (\ln c)$

The initial conditions for ι and $\int \imath \, d\tau$ are the last values of ι and $\int \imath \, d\tau$ from the last phase. The initial value of ζ is $\zeta = 1 + \zeta_f$ where ζ_f is the last length of the focus column, but normalised to z_o, rather than a.

References

1 J W Mather. Phys Fluids, **8**, 366 (1965)

2 S Lee, T Y Tou, S P Moo, M A Eissa, A V Gholap, K H Kwek, S Mulyodrono, A J Smith, Suryadi, W Usada, M Zakaullah. Amer J Phys **56**, 62 (1988)

3 S Lee. Experiments with the ICTP-UM 3.3 kJ Plasma Fusion Facilities. ICTP-H4-SMR554/4 (1991)

4 S Lee. IEEE Trans on Plasma Sc, **19**, 912 (1991)

5 M H Liu, S Lee. SXR Radiation Modelling for Neon Plasma Focus. Intern Congress on Plasma Phys, Prague, June 1998

6 S Lee, P Lee, G Zhang, X Feng, V Gribkov, M Liu, A Serban, T K S Wong. IEEE Trans Plasma Sc, **26**, 1119 (1998)
7 S. Lee & S. H. Saw, Applied Phys Letters **92**, 021503 (2008)
8. S Lee & S. H. Saw. J Fusion Energy. DOI: 10.1007/s10894-008-9132-7, published online: 20 February 2008.
9. S. Lee, S. H. Saw, P. C. K. Lee, R. S. Rawat and H. Schmidt. Computing Plasma Focus Pinch Current from Total Current Measurement; Applied Phys Letters, in production for Vol **92**, Issue 12, 12 March 2008.